Structural and Multidisciplinary Optimization (2024) 67:136
https://doi.org/10.1007/s00158-024-03826-7

RESEARCH PAPER

A smooth maximum regularization approach for robust topology optimization in the ground structure setting

Emily Alcazar[1] · Lorran F. Oliveira[2] · Fernando Vasconcelos Senhora[3] · Adeildo S. Ramos Jr.[2] · Glaucio H. Paulino[1]

Received: 18 September 2023 / Revised: 29 April 2024 / Accepted: 21 May 2024 / Published online: 30 July 2024

Abstract
A robust ground structure topology optimization framework is presented to handle the uncertainty of load direction and design for the worst case compliance scenario. The deterministic optimization framework is formulated by a min-max compliance objective to first determine the critical load angle corresponding to the worst case compliance and then to design the topology for compliance minimization. The first optimization problem, based on our load definition, is shown to be equivalent to a maximum eigenvalue function, thus causing significant drawbacks in gradient-based optimization approaches in the case of eigenvalue coalescence. Here, we propose a method to treat the non-differentiability of the maximum eigenvalue optimization problem by a smooth maximum regularization function; hence, presenting a framework for optimizing ground structure networks considering an infinite number of load directions. The results achieved demonstrate that the proposed framework provides solutions with low compliance in all possible loading directions leading to robust structural designs.

Keywords Topology optimization · Worst case loading · Eigenvalue optimization · Robust topology optimization

1 Introduction

Topology optimization is a method which finds the optimal placement of material and void in a design space under a certain set of design criteria, as originally proposed by Bendsøe and Kikuchi (1988). This method has since become a powerful design tool in several disciplines of engineering to achieve elegant and efficient structures, but in many works has been limited to one or a small, finite number of load case scenarios which may not be fully representative of real-life structural applications (Rozvany 2009; Sigmund and Maute 2013). In topology optimization, when dealing with one particular loading case, the final optimal solution is often extremely sensitive to any perturbation in the loading especially for optimal truss networks such as the Michell structures (Michell 1904). This is due to the optimized structure being highly dependent on the prescribed load case direction as demonstrated in Fig. 1, where a cantilever truss network is optimized for compliance minimization under a single load case in the direction, θ. The results demonstrate the correlation between the applied loading direction and the final number and arrangement of the truss elements as well as the compliance. This example communicates the importance of design approaches that consider many possible loading scenarios for reliable and robust designs; this may include loads varying in magnitude, such as wind or live loads, or loads varying in orientation, such as centripetal forces or vibrational frequencies.

Robust optimization is a class of optimization that deals with uncertainty, which can be handled either by stochastic, deterministic, or worst case approaches (Ben-Tal et al. 2009). In the context of structural design, robust optimization frameworks are important in finding solutions that are resilient in the real-world environment, where uncertainty is present, and can be categorized into subfields namely by reliability-based topology optimization (RBTO) (Kharmanda et al. 2004) and robust topology optimization (RTO)

Responsible editor: Matthew Gilbert

✉ Glaucio H. Paulino
gpaulino@princeton.edu

[1] Department of Civil and Environmental Engineering, Princeton University, Princeton, NJ 08544, USA

[2] Laboratory of Scientific Computing and Visualization Technology Center, Federal Univerity of Alagoas, Maceio, Alagoas 57092-970, Brazil

[3] School of Civil and Environmental Engineering, Georgia Institute of Technology, 790 Atlantic Drive, Atlanta, GA 30332, USA

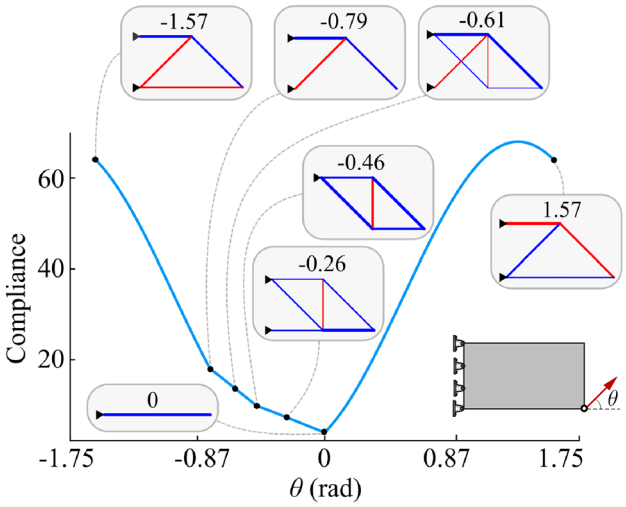

Fig. 1 Multiple topology optimized ground structures with an applied static point load analyzed at varying directions

(Beyer and Sendhoff 2007; Schuëller and Jensen 2008). In this context, RBTO finds the optimal layout of a structure while considering the effects of uncertainty in parameters to avoid a specified failure event, where the optimization framework is composed by expectation functions and failure probabilities (Bae and Wang 2002; Maute and Frangopol 2003; Jensen 2005). For example, RBTO was implemented to incorporate safety into the topology optimization framework through adding randomness in parameters such as geometrical description, material representation, or applied loading in the form of structural reliability constraints which were quantified by a reliability index via first-order reliability methods (Kharmanda et al. 2004). The reliability index approach for quantifying probabilistic constraints has been commonly used for reliability-based structural optimization (Thanedar and Kodiyalam 1992; Reddy et al. 1994; Chandu and Grandhi 1995). Alternatively, RTO aims to design structures that are *robust* in the case of variations in parameters by means of both deterministic and stochastic frameworks (Dunning and Kim 2013; Holmberg et al. 2017; De et al. 2020). Recent works of stochastic RTO include, but are not limited to, accounting for geometric imperfections considering geometric non-linearity by using the perturbation method to quantify stochastic properties (Jansen et al. 2015). Da Silva et al. (2018) presented an RTO framework for minimizing volume subject to local stress constraints written as weighted average between the expected value and standard deviation with uncertainty estimation via the first-order perturbation method. Zhao and Wang (2014) proposed a formulation to minimize compliance considering load uncertainty of both concentrated and uniformly distributed loads, where Monte Carlo simulations are used to approximate the weights required to compute the mean and standard deviation of the compliance before optimization. Deterministic RTO frameworks include a game theory approach proposed by Holmberg et al. (2017) for handling compliance, global stress, or mass as objective functions or constraints in determining the topology for the worst case loading. Senhora et al. (2023) proposed a framework to minimize mass subject to local stress constraints using an augmented Lagrangian method, where the worst case loading was determined using analytical expressions for various different types of loading uncertainty.

For worst case compliance under certain load case parametrization, the min-max formulation has been found to be equivalent to finding a maximum eigenvalue of a generalized eigenvalue problem (Cherkaev and Cherkaev 2008; Holmberg et al. 2017). Eigenvalue problems have been known to arise frequently in structural optimization problems in the form of buckling load factors and vibration frequencies and pose mathematical challenges in the case of multiple eigenvalues for obtaining the sensitivity information (Seyranian et al. 1994). Previous researchers have addressed the convergence issues related to eigenvalue optimization by, but not limited to, semi-definite programming (Ben-Tal and Nemirovski 1997; Holmberg et al. 2015; Thore et al. 2017), adding orthogonal point loads to the RTO framework (Holmberg et al. 2017), using a block Jacobi conjugate gradient iterative approach (Dunning et al. 2016), smooth convex approximation to a composite function of the maximum eigenvalue function (Chen et al. 2004), and using a smoothing method with a projected gradient update scheme for the RTO problem in continuum topology optimization (Nishioka and Kanno 2023).

In this work, we present an RTO formulation for truss structures in the ground structure setting which incorporates load uncertainty via a worst case compliance deterministic approach. The loading parameterization is generalized for a load varying in both magnitude and direction. This framework addresses the issue of optimal truss structures found by traditional topology optimization approaches being highly sensitive to any variation of the applied loading by accounting for infinitely many load directions and designing the topology based on the worst possible loading case. The proposed framework handles the convergence issues related to the maximum eigenvalue optimization problem by the smooth maximum regularization function.

The remainder of this paper is organized as follows: the framework for the load case with uncertain direction is described in a mathematical context in Sect. 2, where a simple truss example is shown to demonstrate the non-smooth sensitivity information that may occur in the maximum eigenvalue problem. The optimization formulation is described in Sect. 3, and in Sect. 4 the sensitivity analysis is derived. The numerical results are shown in Sect. 5, where the framework is demonstrated to find topologies which are

robust with low compliance for varying load directions. The proposed framework is also demonstrated to handle various types of rotating loads. Our findings are concluded in Sect. 6.

2 Maximum eigenvalue function

2.1 Uncertainty loading

In our framework, we approach the RTO via a deterministic approach in finding the critical loading scenario. An infinite number of load cases is considered for the case of a point load varying in $[-\pi, \pi]$ which can be freely rotating or subject to a range of admissible angles. The load cases are parameterized in a manner such that the magnitude can vary as a function of θ; this is done by the following expression:

$$\boldsymbol{F}(\theta) = \boldsymbol{F}_x \cos\theta + \boldsymbol{F}_y \sin\theta, \tag{1}$$

where $\boldsymbol{F}_x$ and $\boldsymbol{F}_y$ are the basis vectors of the load parameterization with the proper corresponding magnitude. The uncertainty of the loading direction is accounted for by the $\cos\theta$ and $\sin\theta$ terms. In the general case when $\|\boldsymbol{F}_x\| \neq \|\boldsymbol{F}_y\|$ the load will take the form of an ellipsoid domain and in the particular case when $\|\boldsymbol{F}_x\| = \|\boldsymbol{F}_y\|$ the load is parameterized by a circular domain. For additional flexibility in the loading, the elliptical load domain may also be subject to an arbitrary rotation, θ_{rot}, by rotating the basis vectors accordingly. The three loading cases mentioned above will be further referenced as an unconstrained loading case. The fourth type of loading case to be considered in this work is when theta is restricted to a range of admissible angles, θ_r. This will be denoted as the constrained loading case. Due to the symmetry of compliance as a result of the linear elasticity, the range of the constrained loading will also contain a secondary range of admissible angles π radians apart. The secondary range of admissible angles is shown in blue in Fig. 2d. The complete set of different loading cases are illustrated in Fig. 2.

From the linear elastic state equation the displacement can be written by

$$\boldsymbol{U}(\boldsymbol{x}, \theta) = \boldsymbol{U}_x(\boldsymbol{x})\cos(\theta) + \boldsymbol{U}_y(\boldsymbol{x})\sin(\theta). \tag{2}$$

The displacement terms are separated by the degrees of freedom associated with the x and y direction and are determined by the stiffness matrix and force vector, $\boldsymbol{U}_x(\boldsymbol{x}) = \left(\boldsymbol{K}(\boldsymbol{x})^{-1}\boldsymbol{F}_x\right)$ and $\boldsymbol{U}_y(\boldsymbol{x}) = \left(\boldsymbol{K}(\boldsymbol{x})^{-1}\boldsymbol{F}_y\right)$. Then the compliance for this load parameterization can then be written as

$$C(\boldsymbol{x}, \theta) = \boldsymbol{U}(\boldsymbol{x}, \theta)^T \boldsymbol{K}(\boldsymbol{x}) \boldsymbol{U}(\boldsymbol{x}, \theta). \tag{3}$$

After distributing the terms, the compliance can be rewritten by the following expression (Senhora et al. 2023):

$$\begin{aligned} C(\boldsymbol{x}, \theta) = \; & t_{xx}(\boldsymbol{x})\cos^2(\theta) + t_{yy}(\boldsymbol{x})\sin^2(\theta) \\ & + 2t_{xy}(\boldsymbol{x})\cos(\theta)\sin(\theta). \end{aligned} \tag{4}$$

The compliance terms are represented by $t_{xx}(\boldsymbol{x}) = \boldsymbol{U}_x^T \boldsymbol{K}(\boldsymbol{x}) \boldsymbol{U}_x$, $t_{yy}(\boldsymbol{x}) = \boldsymbol{U}_y^T \boldsymbol{K}(\boldsymbol{x}) \boldsymbol{U}_y$, and $t_{xy}(\boldsymbol{x}) = \boldsymbol{U}_x^T \boldsymbol{K}(\boldsymbol{x}) \boldsymbol{U}_y$. For demonstration that the optimization problem for finding the critical load angle corresponding to the maximum compliance is equivalent to a maximum eigenvalue problem, we write Eq. 4 in matrix form.

$$\begin{aligned} C(\boldsymbol{x}, \theta) &= \begin{bmatrix} \cos(\theta) & \sin(\theta) \end{bmatrix} \begin{bmatrix} t_{xx} & t_{xy} \\ t_{xy} & t_{yy} \end{bmatrix} \begin{bmatrix} \cos(\theta) \\ \sin(\theta) \end{bmatrix} \\ &= \boldsymbol{n}(\theta)^T \boldsymbol{T}(\boldsymbol{x}) \boldsymbol{n}(\theta) \end{aligned} \tag{5}$$

In our RTO approach for the unconstrained load case, we determine the load direction corresponding to the worst case compliance through the following optimization problem:

$$\begin{aligned} \max_{\boldsymbol{n}} \quad & C(\boldsymbol{x}, \theta) = \boldsymbol{n}(\theta)^T \boldsymbol{T}(\boldsymbol{x}) \boldsymbol{n}(\theta) \\ \text{s.t.} \quad & \boldsymbol{n}(\theta)^T \boldsymbol{n}(\theta) = 1, \end{aligned} \tag{6}$$

where $\boldsymbol{T}(\boldsymbol{x}) \in \mathbb{R}^{n \times n}$ and $\boldsymbol{n}(\theta) \in \mathbb{R}^n$, where n is the spatial dimension. The Lagrangian for this optimization problem can be expressed by

$$\mathcal{L}(\boldsymbol{n}(\theta), \lambda) = \boldsymbol{n}(\theta) \boldsymbol{T}(\boldsymbol{x}) \boldsymbol{n}(\theta) - \lambda\left(\boldsymbol{n}(\theta)^T \boldsymbol{n}(\theta) - 1\right), \tag{7}$$

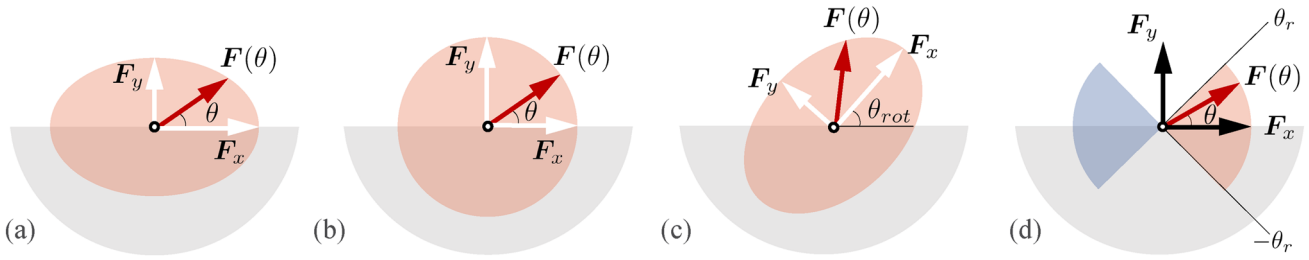

Fig. 2 Illustration of the different load types that may be specified by the general loading definition; **a** the elliptical domain when $\|\boldsymbol{F}_x\| \neq \|\boldsymbol{F}_y\|$; **b** the particular case when $\|\boldsymbol{F}_x\| = \|\boldsymbol{F}_y\|$ for the circular domain; **c** the rotated elliptical domain; **d** the constrained load domain

where λ is the Lagrange multiplier. The Lagrangian is then evaluated at the stationary point.

$$\begin{aligned} &\frac{\partial \mathcal{L}(\boldsymbol{n}(\theta), \lambda)}{\partial \boldsymbol{n}(\theta)} = 0 = 2\boldsymbol{T}(\boldsymbol{x})\boldsymbol{n}(\theta) - 2\lambda \boldsymbol{n}(\theta) \\ &\implies \boldsymbol{T}(\boldsymbol{x})\boldsymbol{n}(\theta) = \quad \lambda \boldsymbol{n}(\theta) \end{aligned} \tag{8}$$

From expression Eq. 8 it is clear that the optimization problem Eq. 6 is an eigenvalue problem and due to the maximization it is equivalent to a maximum eigenvalue function. In the optimization problem the design variable is the eigenvector, $\boldsymbol{n}(\theta)$, which is used to find the maximum associated eigenvalue, λ. Similarly, this same definition for the continuously varying load can be extended to 3-D spherically varying load problems in polar coordinates which is also equivalent to a maximum eigenvalue problem, see Appendix C for details.

For the constrained loading case, delimited by θ_r, the optimization problem changes to the following with an additional constraint on theta.

$$\begin{aligned} \max_{\boldsymbol{n}} \quad & C(\boldsymbol{x}, \theta) = \boldsymbol{n}(\theta)^T \boldsymbol{T}(\boldsymbol{x}) \boldsymbol{n}(\theta) \\ \text{s.t.} \quad & \boldsymbol{n}(\theta)^T \boldsymbol{n}(\theta) = 1 \\ & -\theta_r \leq \theta \leq \theta_r \end{aligned} \tag{9}$$

This may be equivalent to the eigenvalue problem if the range of admissible angles is large enough to capture both eigenvectors.

The eigenvalue information is used to formulate the topology optimization problem, where the structural layout is designed for the worst case loading direction by minimizing the maximum eigenvalue function. The minimization of the maximum eigenvalue function is a special class of eigenvalue optimization problems (Lewis and Overton 1996). These optimization problems obtain difficulties in computing the sensitivity information when the objective function is non-smooth in the case of repeated eigenvalues (Overton and Womersley 1995; Shapiro and Fan 1995). This results in standard approaches of solving optimization problems via gradient-based methods useless as the first-order sensitivity information is inaccurate.

For demonstration let us consider an $n \times n$ real symmetric matrix, $\boldsymbol{A}(\boldsymbol{x})$, which is dependent smoothly on a vector of real parameters $\boldsymbol{x} \in \mathbb{R}^n$. The real eigenvalues are denoted by $\lambda_1(\boldsymbol{x}) \geq \lambda_2(\boldsymbol{x}) \geq ... \geq \lambda_n(\boldsymbol{x})$ in non-increasing order and their corresponding eigenvectors are denoted by $\boldsymbol{v}_1, \boldsymbol{v}_2, ..., \boldsymbol{v}_n$. The eigenvectors will be orthonormal due to the symmetry of $\boldsymbol{A}(\boldsymbol{x})$ as true in the case of linear elasticity. It is assumed that $\boldsymbol{A}(\boldsymbol{x})$ is twice continuously differentiable and thus, when the eigenvalues are simple, i.e., when the eigenvalues correspond to a multiplicity of one, they are Frécher differentiable and inherit C^2 smoothness of the function $\boldsymbol{A}(\boldsymbol{x})$ (Overton and Womersley 1995). The problem can be written such that

$$\boldsymbol{A}(\boldsymbol{x})\boldsymbol{v}_i = \lambda_i \boldsymbol{v}_i \quad i = 1, ..., n. \tag{10}$$

Given that the eigenvectors are orthonormal for the symmetric matrix $\boldsymbol{A}(\boldsymbol{x})$, we may multiply the expression above by $\boldsymbol{v}_j$ to obtain

$$\boldsymbol{v}_i^T \boldsymbol{A}(\boldsymbol{x})\boldsymbol{v}_j = \lambda_i \delta_{ij} \quad i, j = 1, ..., n, \tag{11}$$

where δ_{ij} is the Kronecker delta. From expression Eq. 11 the first-order sensitivities of the eigenvalues may be obtained by

$$\frac{\partial \lambda_i}{\partial x_j} = \boldsymbol{v}_i^T \frac{\partial \boldsymbol{A}(\boldsymbol{x})}{\partial x_j} \boldsymbol{v}_i. \tag{12}$$

The sensitivity for the eigenvalues in Eq. 12 only holds true when the eigenvalue is simple with a multiplicity of one for distinct eigenvalues which additionally implied C^2 continuity such that this specific case of the maximum eigenvalue function can be minimized using conventional gradient-based approaches. However, if the eigenvalues coalesce with a multiplicity of $n > 1$ this indicates that n eigenvalues are equivalent and correspond to eigenvectors that are not unique resulting in an infinite number of solutions that satisfy Eq. 11 through linear combinations of different eigenvectors corresponding to the same repeated eigenvalue (Seyranian et al. 1994). In this case, the expression for the gradient of the eigenvalue in Eq. 12 no longer holds and the eigenvalue is not continuously differentiable.

2.2 Repeated eigenvalue example

To show how repeated eigenvalues may arise in our proposed RTO framework, a simple, symmetric two-variable truss example is presented followed by a discussion on our approach for treating the eigenvalue singularities in our optimization framework.

2.2.1 General case

In Fig. 3, we generalize the parameterized loading case for a simple four bar truss problem, where the cross-sectional areas are denoted by x_1 and x_2, L_1 and L_2 are the lengths of the bars, F_x and F_y are the magnitude of the basis applied loads, and α is the arbitrary angle at which the load basis is positioned.

We arrive at the following composition for the stiffness matrix:

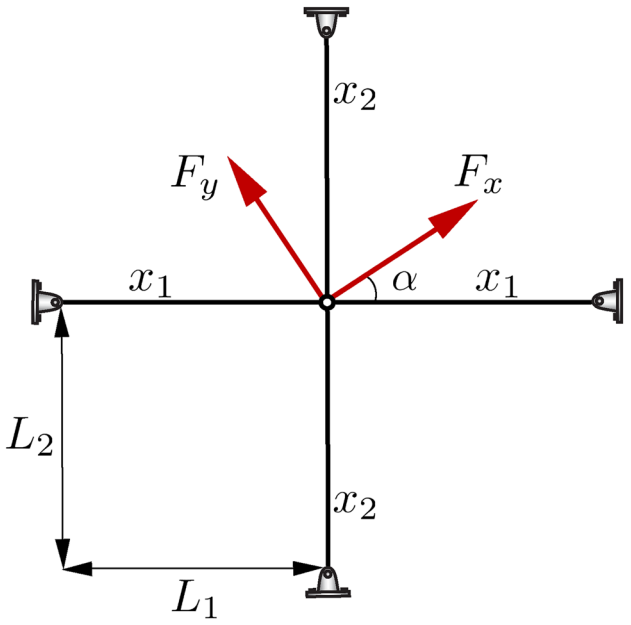

Fig. 3 Generalized truss example demonstrating repeated eigenvalues

$$\boldsymbol{K}(\boldsymbol{x}) = \begin{bmatrix} \frac{2Ex_1}{L_1} & 0 \\ 0 & \frac{2Ex_2}{L_2} \end{bmatrix}, \tag{13}$$

where E is the Young's modulus. For the purpose of this example, we take the external force vector to be expressed by the following definition similarly to Holmberg et al. (2015).

$$\boldsymbol{F}(\alpha, \theta) = \boldsymbol{B}(\alpha)^T \boldsymbol{r}(\theta) \tag{14}$$

In keeping consistency with our previous definition Eq. 1, $\boldsymbol{B}(\alpha)$ represents a matrix where each column corresponds to a basis vector of the load parameterization and $\boldsymbol{r} = [\cos\theta, \sin\theta]^T$ captures the uncertainty in the load direction. Using this definition for $\boldsymbol{F}(\theta)$ the compliance may be defined by

$$C(\boldsymbol{x}, \alpha, \theta) = \boldsymbol{r}(\theta)^T \boldsymbol{B}(\alpha) \boldsymbol{K}(\boldsymbol{x})^{-1} \boldsymbol{B}(\alpha)^T \boldsymbol{r}(\theta). \tag{15}$$

Here, the compliance matrix may be expressed by $\boldsymbol{T}(\boldsymbol{x}, \alpha) = \boldsymbol{B}(\alpha)\boldsymbol{K}(\boldsymbol{x})^{-1}\boldsymbol{B}(\alpha)^T$. For the sake of generalizing the compliance matrix in terms of α, we expand the $\boldsymbol{B}(\alpha)$ matrix by

$$\boldsymbol{B}(\alpha) = \begin{bmatrix} F_x \cos\alpha & F_x \sin\alpha \\ -F_y \sin\alpha & F_y \cos\alpha \end{bmatrix}. \tag{16}$$

Using the new definition of $\boldsymbol{B}(\alpha)$ the compliance matrix $\boldsymbol{T}(\boldsymbol{x}, \alpha)$ is computed,

$$\boldsymbol{T}(\boldsymbol{x}, \alpha) = \begin{bmatrix} t_{xx}(\boldsymbol{x}, \alpha) & t_{xy}(\boldsymbol{x}, \alpha) \\ t_{xy}(\boldsymbol{x}, \alpha) & t_{yy}(\boldsymbol{x}, \alpha) \end{bmatrix} \tag{17}$$

where

$$\begin{aligned} t_{xx}(\boldsymbol{x}, \alpha) &= \frac{F_x^2\left(L_1 x_2 \cos^2(\alpha) + L_2 x_1 \sin^2(\alpha)\right)}{2Ex_1x_2} \\ t_{xy}(\boldsymbol{x}, \alpha) &= \frac{F_x F_y\left(L_1 x_2 - L_2 x_1\right)\sin(2\alpha)}{4Ex_1x_2} \\ t_{yy}(\boldsymbol{x}, \alpha) &= \frac{F_y^2\left(L_1 x_2 \sin^2(\alpha) + L_2 x_1 \cos^2(\alpha)\right)}{2Ex_1x_2}. \end{aligned} \tag{18}$$

By examining the general expression of $T(\boldsymbol{x}, \alpha)$ in Eqs. 17 and 18, it is clear that repeated eigenvalues may arise in the following conditions: (1) when $\alpha = 0$ or $\alpha = n\pi/2$ (n=0,1,2,3...) and $F_x^2 L_1/x_1 = F_y^2 L_2/x_2$; (2) $L_1 x_2 = L_2 x_1$ and $F_x = F_y$.

2.2.2 Particular case

In a particular case study, we examine the compliance matrix when $\alpha = 0$ which results in the following compliance matrix:

$$\boldsymbol{T}(\boldsymbol{x}, 0) = \begin{bmatrix} \frac{L_1 F_x^2}{2Ex_1} & 0 \\ 0 & \frac{L_2 F_y^2}{2Ex_2} \end{bmatrix}. \tag{19}$$

Because $\boldsymbol{T}$ is a diagonal matrix it is observed that the eigenvalues of $\boldsymbol{T}$, $[\lambda_1, \lambda_2] = \text{eig}(\boldsymbol{T})$, are the diagonal entries of $\boldsymbol{T}$ denoted by the following.

$$\lambda_1 = \frac{L_1 F_x^2}{2Ex_1}, \quad \lambda_2 = \frac{L_2 F_y^2}{2Ex_2} \tag{20}$$

For this particular case study it is assumed that $L_1 = L_2$, $F_x = F_y$ and $x_1 = x_2$ which implies that the eigenvalues coalesce and thus are not continuously differentiable. The singularity for this case is also visualized in the contour plot of the compliance objective in Fig. 4, where it can be seen that there exists discontinuities along the axis where $x_1 = x_2$.

2.3 Smooth maximum regularization

If repeated eigenvalues occur in a small truss example it is intuitive that they may arise when dealing with highly dense ground structure networks. To handle the non-smooth eigenvalue function in the gradient-based optimization framework, we approximate the maximum eigenvalue function by a smooth maximum regularization function which we will refer to as the μ-regularization (Biswas et al. 2021). By imposing a

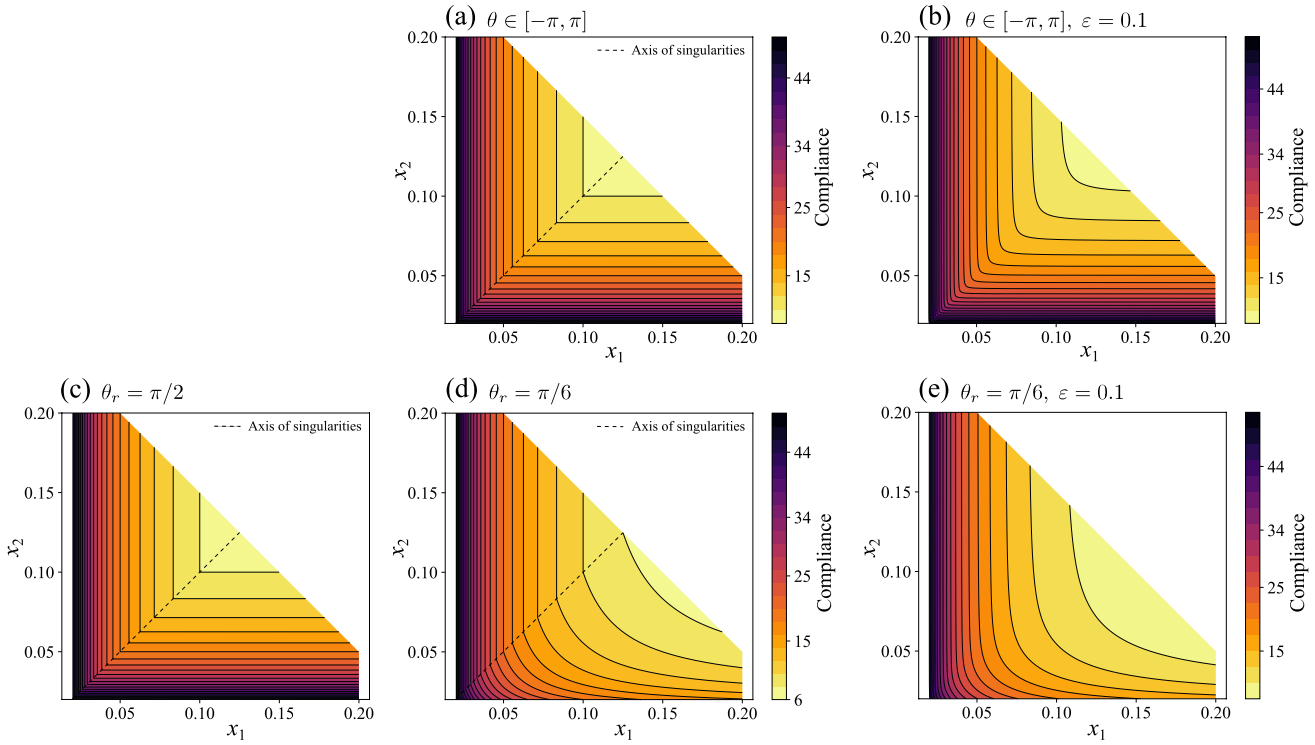

Fig. 4 Contour plot of the compliance objective function of the truss example for the particular case when $\alpha = 0$; **a** the original problem with unconstrained loading and no regularization; **b** the unconstrained loading with μ regularization; **c** the constrained loading case with $\theta_r = \pi/2$ **d** the constrained loading case with $\theta_r = \pi/6$; **e** the constrained loading with μ regularization

smooth regularization function on the maximum eigenvalue function, we resolve any instances of singularities that would arise in the original non-smooth function. Thus, alleviating convergence issues caused by invalid gradient information and oscillatory behavior between the orthogonal worst case loading directions. The proposed μ-regularization uses information from both eigenvalues to approximate and smooth the maximum eigenvalue function, which approaches the original function as $\mu \to 0$, where μ is a parameter of the same units of the eigenvalues. Alternatively, one could also use other regularization functions to achieve this outcome, this is demonstrated for the p-norm regularization function in Appendix B.

$$\max(\lambda_1, \lambda_2) \approx f_\mu(\lambda_1, \lambda_2) = \frac{1}{2}(\lambda_1 + \lambda_2 + \sqrt{(\lambda_1 - \lambda_2)^2 + \mu^2}) \tag{21}$$

Even in the case that the eigenvalue functions are non-smooth upon eigenvalue coalescence their summation and product may be represented by smooth functions by the following remarks:

Remark 1 Considering a real 2×2 symmetric, non-singular, matrix $\boldsymbol{A}(\boldsymbol{x})$ depending smoothly on parameter $\boldsymbol{x}$ with an orthonormal basis of eigenvectors for all $x \in \mathbb{R}^n$; the sum and product of the eigenvalues may be expressed by smooth functions: $\lambda_1(\boldsymbol{x}) + \lambda_2(\boldsymbol{x}) = \mathrm{tr}\boldsymbol{A}(\boldsymbol{x})$ and $\lambda_1(\boldsymbol{x})\lambda_2(\boldsymbol{x}) = \det\boldsymbol{A}(\boldsymbol{x})$ which holds for changes in multiplicity. Thus, the derivative of the eigenvalue summation and products exist as proved in Gravesen et al. (2011).

To show that the sensitivity of the proposed μ-regularization function is composed of smooth functions of the eigenvalues, we take the derivative of the function in a general way.

$$\frac{d}{d\boldsymbol{x}}[f_\mu(\lambda_1(\boldsymbol{x}), \lambda_2(\boldsymbol{x}))] = \frac{\partial f_\mu}{\partial \lambda_1}\frac{\partial \lambda_1}{\partial \boldsymbol{x}} + \frac{\partial f_\mu}{\partial \lambda_2}\frac{\partial \lambda_2}{\partial \boldsymbol{x}} \tag{22}$$

The partial derivatives of the μ-regularization function with respect to the eigenvalues are derived as follows:

$$\frac{\partial f_\mu}{\partial \lambda_1} = \frac{1}{2} + \frac{\lambda_1 - \lambda_2}{2\sqrt{(\lambda_1 - \lambda_2)^2 + \mu^2}} \tag{23}$$

$$\frac{\partial f_\mu}{\partial \lambda_2} = \frac{1}{2} + \frac{\lambda_2 - \lambda_1}{2\sqrt{(\lambda_1 - \lambda_2)^2 + \mu^2}} \quad . \tag{24}$$

When the eigenvalues are equivalent we can make the claim that $\partial f_\mu/\partial \lambda_1 = \partial f_\mu/\partial \lambda_2 = 1/2$, which leads to Eq. 22 being

represented in a simplified form for the repeated eigenvalue case by

$$\frac{d}{d\boldsymbol{x}}[f(\lambda_1(\boldsymbol{x}),\lambda_2(\boldsymbol{x}))] = \frac{1}{2}\left(\frac{\partial\lambda_1}{\partial\boldsymbol{x}} + \frac{\partial\lambda_2}{\partial\boldsymbol{x}}\right). \tag{25}$$

Thus in addition to the μ-regularization function being composed by sum and product terms of the eigenvalues, the derivative of the μ-regularization function in the case of repeated eigenvalues is composed by the derivative of the summation of eigenvalues with respect to $\boldsymbol{x}$ which is proven to exist by the earlier Remark 1.

Corollary 1 *Given that $f_\mu(\lambda_1,\lambda_2)$ is a smooth function and is composed by smooth functions for λ_1 and λ_2, even in the occurrence of repeated eigenvalues, the derivative of $f_\mu(\lambda_1,\lambda_2)$ is continuous and may be expressed by Eq. 26.*

$$\frac{\partial f_\mu(\boldsymbol{x})}{\partial\boldsymbol{x}} = \frac{1}{2}\left(\frac{\partial\lambda_1}{\partial\boldsymbol{x}} + \frac{\partial\lambda_2}{\partial\boldsymbol{x}} + \left((\lambda_1-\lambda_2)^2+\mu^2\right)^{-1/2} (\lambda_1-\lambda_2)\left(\frac{\partial\lambda_1}{\partial\boldsymbol{x}} - \frac{\partial\lambda_2}{\partial\boldsymbol{x}}\right)\right) \tag{26}$$

The $\partial\lambda_i/\partial x_j$ terms can be determined by equation 12 as long as the basis of eigenvectors is orthonormal (Torii and Faria 2017), which is true in the case of linear elasticity due to the symmetric stiffness matrix. Thus, the μ-regularization function is continuously differentiable for repeated eigenvalues. This approach is suitable for changes in multiplicity throughout the optimization and is computationally inexpensive since the worst case loading framework only deals with symmetric matrices of dimensions $n\times n$ with $n=2$ for 2D structures.

To demonstrate that the μ-regularization approach does smooth the singularities for the unconstrained loading problem and more closely approximates the original eigenvalue function as $\mu\to 0$, we impose the regularization onto the original simple truss example with $\epsilon = 0.1$ (see Eq. 33 for more details). In Fig. 4a, b, the contour plot of the μ regularized compliance objective function and the original, non-regularized compliance is shown. The original compliance function at $x_1 = x_2$ is non-smooth which indicates that the derivative of compliance is not continuous as the directional derivative varies depending on which side the limit is taken from. For the compliance which is approximated by μ-regularization, the function is continuous and smooth and more closely approximates the original function as $\mu\to 0$. The same regularization approach is imposed on the constrained loading framework to achieve smoothness. In Fig. 4c, we show the original non-smooth problem when $\theta_r = \pi/2$ is equivalent to that of the unconstrained framework in (a). We also demonstrate in part (d) that the non-smoothness arises even for a constraint that does not contain both eigenvalues, for the case, where $\theta_r = \pi/6$, due to the discrete bound on θ. We then show in part (e) that after imposing regularization we can achieve a smooth function for the $\theta_r = \pi/6$ case. Both proposed topology optimization frameworks for unconstrained and constrained loading will include μ–regularization to make the problem well–posed for gradient-based optimization.

3 Optimization formulation

3.1 Unconstrained loading

The RTO framework presented in this work is described by the following min-max optimization formulation.

$$\min_{\boldsymbol{x}}\max_{\boldsymbol{\theta}} \quad C(\boldsymbol{x},\boldsymbol{\theta}) \tag{27}$$

To formulate a topology optimization framework that considers the critical load case directions for the unconstrained load, the critical load case directions (eigenvectors) corresponding to the maximum and minimum compliance (eigenvalues) are determined and used to inform the topology optimization statement at each iteration. To avoid issues related to eigenvalue coalescence both eigenvalue information is used for the formulation of the compliance minimization objective function using the μ–regularization function as shown in Eq. 28 and discussed in Sect. 2. The topology optimization procedure for the presented min-max formulation is outlined in Algorithm 1.

Algorithm 1

For the iteration $k=0$, set an initial design variable guess for $\boldsymbol{x}^0$
while $k <$ maxIter and $\Delta x >$ tol **do**
  Set $k = k+1$
  Conduct FEA to setup worst case compliance problem
  Find critical load directions $\boldsymbol{\theta}^{*,k}$ by $\max_{\boldsymbol{\theta}} C(\boldsymbol{x}^{k-1},\boldsymbol{\theta})$
  Formulate the objective function using $\boldsymbol{\theta}^{*,k}$ in $C(\boldsymbol{x},\boldsymbol{\theta}^{*,k})$
  Determine $\boldsymbol{x}^k$ by solving for one iteration of $\min_{\boldsymbol{x}\in\mathcal{X}} C(\boldsymbol{x},\boldsymbol{\theta}^{*,k})$ using the OC update scheme
  Compute $\Delta\boldsymbol{x} = \max\left(\left|\frac{\boldsymbol{x}^k-\boldsymbol{x}^{k-1}}{(1+\boldsymbol{x}^{k-1})}\right|\right)$
  if stopping criteria is satisfied **then**
    break
  end if
end while

Due to the linear elasticity, the compliance matrix $\boldsymbol{T} \in \mathbb{R}^{nxn}$ is positive semi-definite and symmetric, with eigenvalues $\lambda \in \mathbb{R}^{+}$ and orthogonal eigenvectors. We denote the eigenvalues by $[C_{max}, C_{min}] = \text{eig}(\boldsymbol{T})$ which are then used to inform the topology optimization problem. To visualize the previous remarks on the relation of the eigenvalues to the best and worst case compliance, the compliance function, $C(\boldsymbol{x}, \boldsymbol{\theta})$, is plotted in Fig. 5. The figure demonstrates the periodicity of the function, the orthogonality of the eigenvectors, and the relation of the eigenvalues to the compliance extrema.

The topology optimization problem is composed by the smooth μ−regularization with both eigenvalues as entries $C_{min}(\boldsymbol{x}, \theta_{min}^{cr})$ and $C_{max}(\boldsymbol{x}, \theta_{max}^{cr})$, which will be denoted by C_{min} and C_{max} for brevity.

$$\begin{aligned} \min_{\boldsymbol{x}} \quad & C(\boldsymbol{x}, \boldsymbol{\theta}) = \frac{1}{2}\Big(C_{max} + C_{min} \\ & + \sqrt{(C_{max} - C_{min})^2 + \mu^2}\Big) \\ \text{s.t.} \quad & g(\boldsymbol{x}) = \boldsymbol{L}^T \boldsymbol{x} - V_{max} \leq 0 \\ & x_{min} \leq x^i \leq x_{max} \quad i = 1, ..., n \\ \text{with} \quad & \boldsymbol{K}(\boldsymbol{x})\boldsymbol{u}(\boldsymbol{x}, \boldsymbol{\theta}) = \boldsymbol{F}(\boldsymbol{\theta}) \end{aligned} \tag{28}$$

The objective function now has influence from both eigenvalue and eigenvector information such that if there are repeated eigenvalues, the μ-regularization function will approximate the maximum of them. The design variables for the minimum compliance problem are the cross-sectional areas, $\boldsymbol{x}$, which appear in the eigenvalue terms. The objective function is subject to a volume constraint, where V_{max} is an arbitrarily set maximum volume and $\boldsymbol{L}$ is the vector of bar lengths. Box constraints are also imposed on the cross-sectional areas by x_{min} and x_{max} for n number of bars. The lower bound of the box constraints, x_{min}, is set to be a small value greater than zero such that the stiffness matrix never becomes singular during the optimization. Linear elastic state equations are imposed and defined by the stiffness matrix $\boldsymbol{K}(\boldsymbol{x})$, external force vector $\boldsymbol{F}(\boldsymbol{\theta})$, and the implicitly determined displacement $\boldsymbol{u}(\boldsymbol{x}, \boldsymbol{\theta})$.

3.2 Constrained loading

For the loading case constrained by θ_r , we propose a framework that smooths instances of singularities through the same μ regularization defined previously. However, in this case, the definition for C_{max} and C_{min} is modified to obtain the appropriate maximum and minimum compliance for the range of admissible angles. This is achieved by first computing the analytical direction for the unbounded maximum compliance by

$$\theta_1^{cr} = \tan^{-1}(2t_{xy}, t_{xx} - t_{yy}), \tag{29}$$

(see Senhora et al. (2023) for more details) and the direction corresponding the unbounded minimum compliance

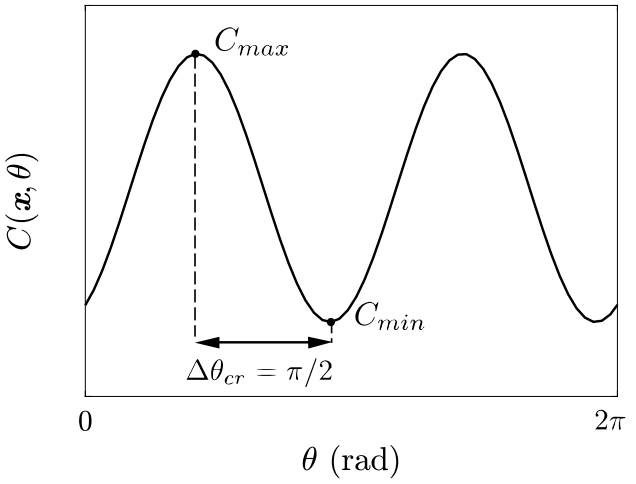

Fig. 5 Compliance as a function of theta where the eigenvalues correspond to the maximum and minimum compliance with orthogonal eigenvectors

$$\theta_2^{cr} = \theta_1^{cr} - \frac{\pi}{2}\,\text{sign}\,(\theta_1^{cr} + \phi), \tag{30}$$

where ϕ is a "machine epsilon" value to ensure the term inside the sign operator is non-zero. Note that these equations are equivalent to finding the direction of the eigenvectors. To now consider the constraint on our loading direction, we find the corresponding maximum and minimum compliance within the loading range as follows:

$$\theta_{max}^{cr} = \min\left(\max\left(\theta_1^{cr}, -\theta_r\right), \theta_r\right) \tag{31}$$

$$\theta_{min}^{cr} = \min\left(\max\left(\theta_2^{cr}, -\theta_r\right), \theta_r\right) \quad . \tag{32}$$

With the new critical loading directions for the constrained case, we may formulate our topology optimization problem equivalently to Eq. 28, where the C_{max} and C_{min} are determined by the directions defined in Eqs. 31 and 32.

In the proposed objective function, we compute the regularization parameter by a general approach.

$$\mu = \varepsilon\left(\frac{C_{max}^0 + C_{min}^0}{2}\right) \tag{33}$$

The parameter ε is a sufficiently small parameter ($\varepsilon = 0.05$ in this work) and the terms C_{max}^0 and C_{min}^0 correspond to the eigenvalues at the first iteration of the topology optimization procedure. This was the approach used to compute the μ across all numerical examples.

4 Sensitivity analysis

In order to solve the topology optimization problem, we use gradient-based solvers which require accurate gradient information of both the objective and the constraint functions. We begin the sensitivity analysis by taking the derivative of the volume constraint.

$$\frac{dg(\boldsymbol{x})}{dx_i} = L_i, \quad i = 1, ..., n \tag{34}$$

Next the sensitivity of the objective function is written in a general form derived by the chain rule:

$$\frac{dC(\boldsymbol{x}, \boldsymbol{\theta})}{d\boldsymbol{x}} = \frac{\partial C}{\partial \boldsymbol{x}} + \frac{\partial C}{\partial \boldsymbol{\theta}} \frac{\partial \boldsymbol{\theta}}{\partial \boldsymbol{x}}. \tag{35}$$

For the unconstrained loading case, the C_{max} and C_{min} eigenvalues will always be at stationary points and thus $\partial C/\partial \boldsymbol{\theta} = 0$ which cancels the $\partial \boldsymbol{\theta}/\partial \boldsymbol{x}$ term. For the constrained loading case, where the critical directions lie on the bound, the $\partial \boldsymbol{\theta}/\partial \boldsymbol{x} = 0$ due to θ_r being independent of $\boldsymbol{x}$. In the case that the critical load directions are within the bound this implies the $\partial C/\partial \boldsymbol{\theta} = 0$ as in the unconstrained case. For both loading scenarios our total derivative becomes $dC(\boldsymbol{x}, \boldsymbol{\theta})/d\boldsymbol{x} = \partial C/\partial \boldsymbol{x}$, with the sensitivity of the objective function by

$$\begin{aligned} \frac{dC(\boldsymbol{x}, \boldsymbol{\theta})}{d\boldsymbol{x}} &= \frac{\partial C}{\partial \boldsymbol{x}} \\ &= \frac{1}{2}\left[\frac{\partial C_{max}}{\partial \boldsymbol{x}} + \frac{\partial C_{min}}{\partial \boldsymbol{x}}\right. \\ &\quad + \left((C_{max} - C_{min})^2 + \mu^2\right)^{-1/2} (C_{max} - C_{min}) \\ &\quad \left.\left(\frac{\partial C_{max}}{\partial \boldsymbol{x}} - \frac{\partial C_{min}}{\partial \boldsymbol{x}}\right)\right]. \end{aligned} \tag{36}$$

The sensitivities of the maximum and minimum compliance terms may be determined by equation 11 as per discussion in Sect. 2. We note that compliance terms may be expressed in terms of the cross-sectional areas and the corresponding loading direction by

$$C_{max}(\boldsymbol{x}, \theta_{cr}^{max}) = \boldsymbol{F}^T(\theta_{cr}^{max}) \boldsymbol{U}(\boldsymbol{x}, \theta_{cr}^{max}), \tag{37}$$

where its derivative $\partial C_{max}/\partial \boldsymbol{x}$ is determined by the direct method.

$$\frac{\partial C_{max}}{\partial \boldsymbol{x}} = -\boldsymbol{U}(\boldsymbol{x}, \theta_{cr}^{max})^T \frac{\partial K(\boldsymbol{x})}{\partial \boldsymbol{x}} \boldsymbol{U}(\boldsymbol{x}, \theta_{cr}^{max}) \tag{38}$$

The $\partial C_{min}(\boldsymbol{x}, \theta_{cr}^{min})/\partial \boldsymbol{x}$ term is expressed similarly.

5 Numerical results

In this section, several numerical examples are presented to demonstrate the results achieved by the proposed optimization framework. In the first example, the topology and compliance of the proposed RTO scheme is compared against nominal cases considering a single load direction. In the following example, the significance of the proposed RTO framework is demonstrated by conducting a forward analysis and comparing the results of a truss network designed for a single load direction versus the presented infinite load cases for a point load with $\theta \in [-\pi, \pi]$. Next the third example demonstrates the control of the proposed loading parameterization to handle different shapes of elliptical loading, which result in drastically different structural layouts and designs of the tower domain. The case of multiple rotating point loads is also analyzed in the Disk domain example which examined several cases of multiple point loads including one with repeated eigenvalues. Then we apply a distributed rotating load on the hook domain with our proposed layout constraint in the ground structure setting. Finally, we showcase an example using the proposed framework for the constrained loading case.

The input optimization parameters are summarized in individual tables for each numerical example. The convergence tolerance is the *tol* parameter described in Algorithm 1 and the move limit, γ, controls the allowable update in the design variables at each iteration, see Bendsoe and Sigmund (2013) for more details. The Young's modulus, E, is defined such that the objective function is on the order of magnitude one-ten for efficient performance of the update scheme. All illustrated examples have the same post-processing procedure which includes filtering out the areas that obtain a fraction relative to the maximum area that is below the specified end filter, α_f.

$$x_i = Filter(\boldsymbol{x}, \alpha_f) = \begin{cases} 0 & \text{if } \dfrac{x_i}{\max(\boldsymbol{x})} < \alpha_f \\ x_i & \text{otherwise} \end{cases} \tag{39}$$

If hanging bars remain after the filtering, i.e., bars only connected to the structure by one node, they are subsequently removed from the structure as they do not contribute to the stiffness of the structure. The end filter is chosen to be sufficiently small such that the structure remains in equilibrium. All ground structures meshes are generated with full-level connectivity but the Hook example, and the Circular domain example, see problem description for more details. Finally, all numerical examples considering the unconstrained loading case use the Optimality Criterion method (OC) as the update scheme (Bendsøe 1995) due to

the speed and smooth convergence. The constrained loading range (delimited by θ_r) example uses a globally convergent version of the Method of Moving Asymptotes (MMA) (Svanberg 2002) from the NLOpt package (Johnson 2007) to handle non-monotonic behavior of the θ^{cr}_{max} oscillating on the bound.

5.1 Beam with central loading

In this example, a beam supported on both ends with a load applied to the center is optimized both considering the proposed RTO framework and for the conventional compliance minimization topology optimization considering a single load with a static direction, which we will denote as the nominal case. The beam dimensions are $L_x = 8$ and $L_y = 4$ with spacing discretization between the nodes in the x and y direction as, $N_x = 4$ and $N_y = 4$, resulting in a ground structure with 200 elements. In the RTO framework, the applied rotating load is circular with $\|\boldsymbol{F}_x\| = \|\boldsymbol{F}_y\|$. Other details regarding the optimization input parameters can be seen in Table 1.

It is observed that the RTO framework results in a stable structure unlike some of the solutions of the nominal cases e.g. $\theta = \pm 0.46$, which illustrates additional motivation to account for the worst case loading direction in ground structure optimization. In Fig. 6, the compliance solution is shown for multiple nominal cases of different static directions; each point corresponding to an individual topology optimization problem. The result obtained by the proposed RTO framework is also shown varying as a function of θ. When designing for the nominal case, the compliance result will be more efficient than the result obtained by the RTO case as demonstrated in Fig. 6. However, because those structures were only designed for a single load case direction they will have significantly worse performance for other load directions, which can intuitively be seen by examining the final topologies. However, the topology for the RTO case is a robust design that has improved compliance performance for all possible load directions. This claim is further corroborated in the following example.

5.2 Square domain with central loading

In this example, a square domain is examined for two cases: 1) compliance minimization subject to a single load case with direction $\theta = 3\pi/2$ (nominal case) and 2) a point load with infinitely many loading directions for $\theta \in [-\pi,\ \pi]$ covering a circular domain, $\|\boldsymbol{F}_x\| = \|\boldsymbol{F}_y\|$. The square domain has dimensions of $L = 4$ and the ground structure is generated with $N_x = 32$ and $N_y = 16$ discretization of the nodes. The results are then analyzed for both cases to evaluate the performance of both structures under the point load of varying direction and to illustrate the importance of designing for the critical load case scenario. The final structures are plotted in Fig. 7b, c, where the colors and thickness of the bars are associated with the normalized cross-sectional area. The initial parameters for this study are shown in Table 2.

Table 1 Topology optimization parameters for Beam domain

Elastic modulus, E	1.0
Number of GS bars, N_{bar}	200
Initial area, x_{ini}	0.0346
Maximum area, x_{max}	0.074
Minimum area, x_{min}	0.0013
Volume limit, V_{max}	1.0
Move parameter, γ	1.3287×10^{-5}
Convergence tolerance	1×10^{-8}
End filter, α_f	0.001

Observing the topology resulting from both load cases, we notice a distinct difference in the structure. While the volume constraints are always active and equal for both cases, the nominal case has fewer and thicker members, while the RTO load case has greater and thinner members distributed over the entire domain. It is discovered that the RTO framework will result in a more complex structure design than the nominal case due to considering changing load direction in the optimization objective. When designing for a single load case, see Fig. 7b, the final compliance is $C_s = 1.5222$ with bars arranged to redistribute the force caused by the applied downward vertical load. In this structure, the bars are optimized and eliminated to place more cross-sectional area in the bars that are most important for this one loading condition. In contrast, when observing the topology designed for the square domain considering an applied point load ranging from $\theta \in [-\pi,\ \pi]$, (Fig. 7c), the final structure contains many members which are optimally placed for maximizing stiffness for the critical load case directions of the structure. For this problem, the final eigenvalues were $C_{max} = 1.9187$ and $C_{min} = 1.0869$ with corresponding critical directions of $\theta^{cr}_{max} = -\pi/2$ and $\theta^{cr}_{min} = 0$.

By designing the structure for the critical load case directions at each iteration of the design, the structure will automatically obtain reduced compliance for the other load directions. We can make sense of this mathematically by observing that the critical load case directions correspond to the extrema of the compliance function (see Fig. 5), because the extrema of compliance are minimized, the values in between the extrema will also be reduced due to the continuity of the function. To illustrate this, the final topology is extracted for both loading cases and is subject to a forward analysis to analyze the compliance performance for a point load with varying direction $\theta \in [-\pi,\ \pi]$. As shown in Fig. 7d, the compliance for most of the load directions is significantly lower for the structure designed for to RTO case (red) than that of the structure

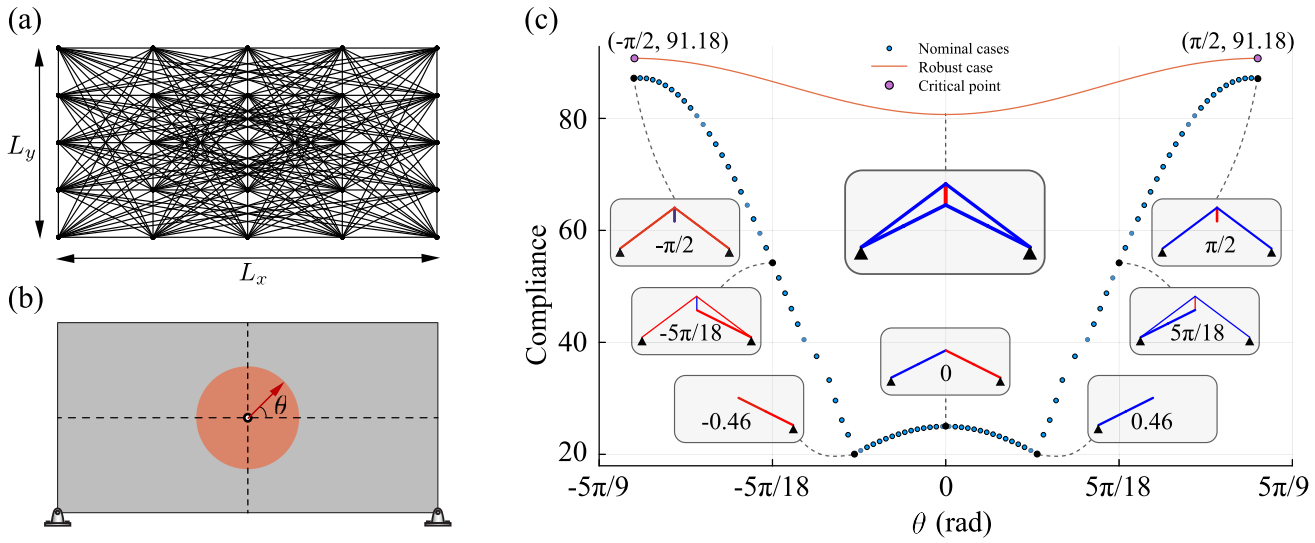

Fig. 6 Depiction of beam with central loading. (a) ground structure generation for the rectangular domain; (b) loading and boundary conditions on the beam domain; (c) optimal topologies with bars in compression (red) and bars in tension (blue) and the final compliance of the proposed robust case versus the nominal cases

Table 2 Topology optimization parameters for square domain

Elastic modulus, E	1×10^5
Number of GS bars, N_{bar}	35,368
Initial area, x_{ini}	4.6068×10^{-8}
Maximum area, x_{max}	4.6068×10^{-4}
Minimum area, x_{min}	4.6068×10^{-12}
Volume limit, V_{max}	0.0018
Move parameter, γ	4.6068×10^{-4}
Convergence tolerance	1×10^{-8}
End filter, α_f	0.002

designed by the nominal case (blue). Only at the direction $\theta = n\pi/2$ with $n \in \mathbb{Z}$ does the single load case have slightly better compliance performance and that is due to it being the load case that was considered during optimization, see Fig. 7e. This corroborates our earlier remarks that even small changes in the applied loading direction can cause significant decrease in the structural performance, which motivates the importance for considering the critical load case direction in the topology optimization framework.

5.3 Tower under elliptical load cases

This following example aims to demonstrate the influence of the shape of the infinite loading domain on the topology by considering the same ground structure subject to two different elliptical loading cases. The first elliptical loading case is defined by the basis vectors $\boldsymbol{F}_x = [5,\ 0]^T$ and $\boldsymbol{F}_y = [0,\ 1]^T$ and the latter is defined by $\boldsymbol{F}_x = [1,\ 0]^T$ and $\boldsymbol{F}_y = [0,\ 5]^T$. The elliptical load cases are subject on the center node on top of the tower domain; the domain has dimensions of $L_x = 2$ and $L_y = 6$ with nodal discretizations of $N_x = 6$ and $N_y = 36$. The optimization parameters are shown in Table 3.

The optimized structures corresponding to the applied elliptical load case are shown in Fig. 8. The results obtained by the first elliptical loading in Fig. 8a have a final compliance of $C_{max} = 14.1337$ and $C_{min} = 0.1833$, which are associated to the critical load case directions of $\theta^{cr}_{max} = 0$ and $\theta^{cr}_{min} = -\pi/2$. The critical load case direction that is associated with the worst case compliance is in the direction, where the elliptical load has the largest magnitude, as expected. For the second elliptical loading problem, Fig. 8b, the compliance results are $C_{max} = 0.8146$ and $C_{min} = 0.7595$ corresponding to directions $\theta^{cr}_{max} = \pi/2$ and $\theta^{cr}_{min} = 0$. In this example, the critical load direction also corresponds to the maximum loading magnitude, however, the critical compliance values are closer together in magnitude, which highlights the importance of considering both critical compliance in the objective function. The flexibility of the loading parametrization is demonstrated in this example where it is shown that changes in the loading basis vectors can cause significant differences in the final topology.

5.4 Disk with multiple varying loads

In this example, we demonstrate the generality of the framework in allowing for multiple point loads varying in the same direction. We take advantage of this feature and examine the significance of multiple varying point loads on a domain by analyzing two cases of the disk domain:

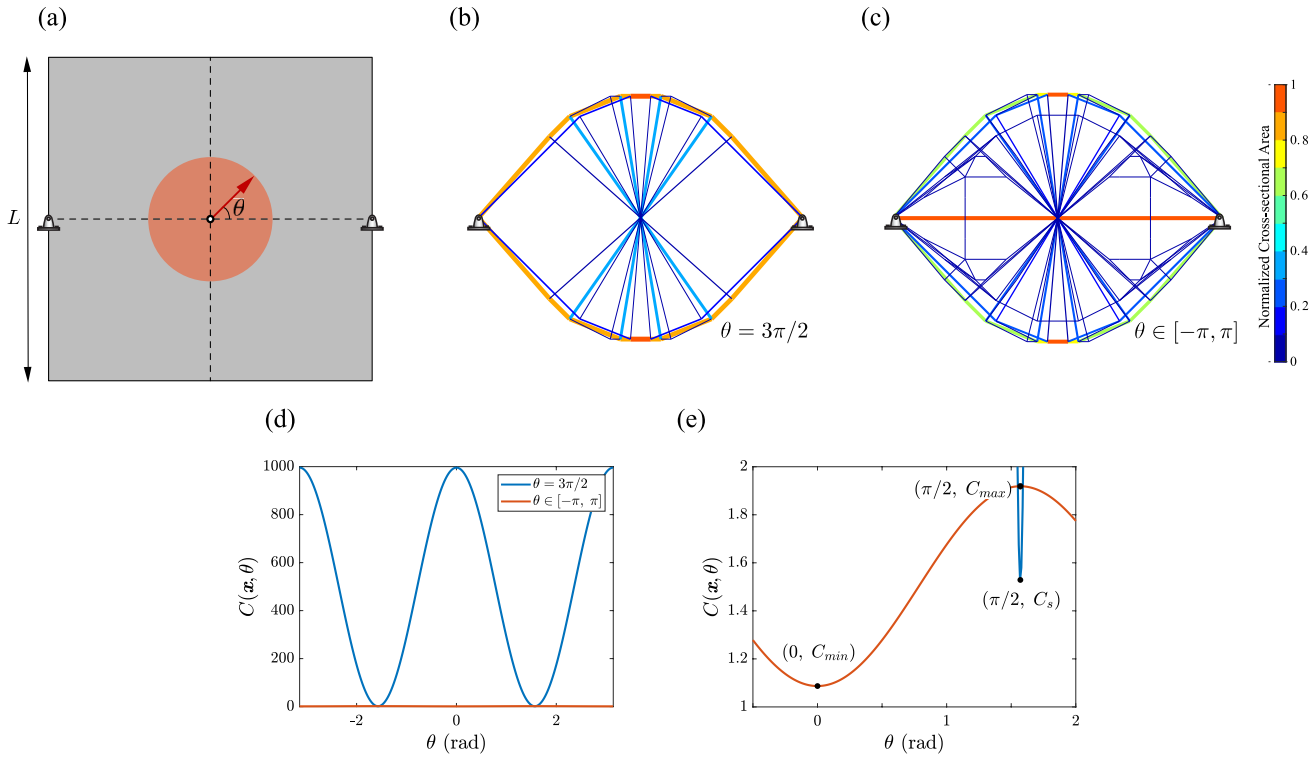

Fig. 7 Illustration of the square domain example examining the results achieved by accounting for a single load case versus the infinite load case. **a** The square domain with a circular load domain located in the center; **b** topology achieved by considering a single load case, where $\theta = 3\pi/2$; **c** topology achieved by the proposed framework considering a circular load case $\theta \in [-\pi, \pi]$; **d** forward analysis of the extracted topologies; **e** close-up of the minimum compliance of the static case and the extrema of the infinite load case

Table 3 Topology optimization parameters for the Tower

Elastic modulus, E	1×10^6
Number of GS bars, N_{bar}	11,526
Initial area, x_{ini}	8.6324×10^{-8}
Maximum area, x_{max}	8.6324×10^{-4}
Minimum area, x_{min}	8.6324×10^{-12}
Volume limit, V_{max}	0.0013
Move parameter, γ	8.6324×10^{-6}
Convergence tolerance	1×10^{-8}
End filter, α_f	0.0012

(1) the disk domain subject to two varying point loads and (2) the disk domain subject to four varying point loads, see Fig. 9 for details. We also examine the influence of changing the magnitude of $\boldsymbol{F}_y$ in four examples, see Figs. 10 and 11 for the loading cases. This study allows us to demonstrate the validity of our approach in solving the maximum eigenvalue optimization problem with smooth convergence. The disk domain is defined to have an outer radius, $r_1 = 100$ and an inner radius, $r_2 = 20$ with all nodes laying on the inner radius fixed. The optimization input parameters can be seen in Table 4.

The final objective values are summarized in Table 5, where the left most column describes the loading conditions for Cases 1 and 2 as described in their corresponding Figs. 10 and 11. For case 1 it is observed that as the load magnitude increases so does the height of the structure, as seen in Fig. 10, to account for the y-direction component of the critical direction. For case 2, we notice a significant change in the geometric layout of the truss bars as the elliptical load domain varies. When the load domain becomes circular at $\|\boldsymbol{F}_x\| = \|\boldsymbol{F}_y\|$, the eigenvalues coalesce during optimization due to the symmetry of the domain and loading conditions. We observe that even during eigenvalue coalescence we achieve smooth convergence of our objective function, see Fig. 12. This particular case demonstrates the efficiency of the proposed formulation to handle repeated eigenvalues and converge to a result that takes both critical loading directions into consideration.

5.5 Hook with distributed load

The Hook example aims to showcase the proposed framework for a distributed rotating load varying with the same θ with $\boldsymbol{F}_x = [1/100, 0]^{\mathrm{T}}$, and $\boldsymbol{F}_y = [0, -1/25]^{\mathrm{T}}$ on an engineering domain. A hook domain is examined with a ground structure mesh generated by GRAND with level-one

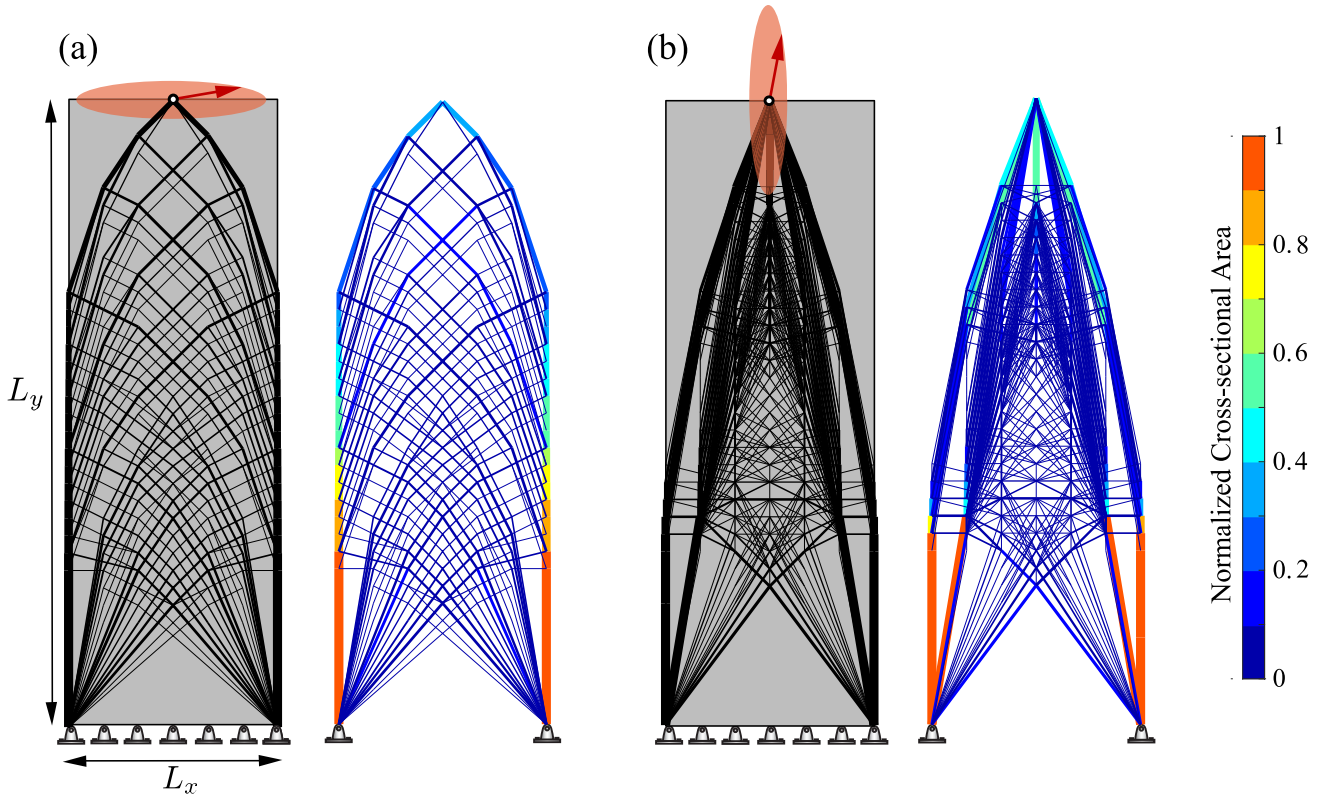

Fig. 8 Tower domain subject to an elliptical load case. **a** Elliptical load case I and the resulting topology; **b** Elliptical load case II and the final topology

Table 4 Topology optimization parameters for the disk domain

Elastic modulus, E	1×10^4
Number of GS bars, N_{bar}	1,116
Initial area, x_{ini}	4.8020×10^{-5}
Maximum area, x_{max}	4.8020×10^{-1}
Minimum area, x_{min}	4.8020×10^{-9}
Volume limit, V_{max}	4.44
Move parameter, γ	4.8020×10^{-5}
Convergence tolerance	1×10^{-6}
End filter, α_f	0.002

connectivity (Zegard and Paulino 2014). To generate solutions that are practical from a manufacturing sense, layout constraints are imposed on the bars to enforce regions where all the bars must have the same cross-sectional area. The optimization parameters for this problem are found in Table 6.

5.5.1 Layout constraint

The layout constraint implementation here is based off previous work in the continuum setting, which imposed pattern gradation through layout constraints (Stromberg et al. 2011). To enforce layout constraints in the ground structure setting, we rewrite the formulation in terms of the auxiliary variables $\boldsymbol{y}$, which serve as the new design variables for the layout constraint framework. The design variables of the original formulation, $\boldsymbol{x}$, are written as a function of a reduced vector of auxiliary variables, $\boldsymbol{y}$, using a transformation matrix $\boldsymbol{P}$. The optimization problem is written as follows:

$$\begin{aligned} \min_{\boldsymbol{y}} \quad & C(\boldsymbol{x}(\boldsymbol{y})) = \boldsymbol{F}^\top \boldsymbol{u}(\boldsymbol{x}(\boldsymbol{y})) \\ \text{s.t.} \quad & \boldsymbol{L}^\top \boldsymbol{x}(\boldsymbol{y}) - V \leq 0 \\ & y_{min} \leq y_i \leq y_{max} \end{aligned}, \tag{40}$$

where

$$x(\boldsymbol{y}) = \boldsymbol{P}\boldsymbol{y}. \tag{41}$$

The transformation matrix $\boldsymbol{P}$ is a binary matrix that maps each element of the vector $\boldsymbol{y}$ to a single element of the vector $\boldsymbol{x}$. This implies that the box constraints are equivalent for both variables. For more information on the sensitivity analysis of this framework see Appendix D.

To illustrate the application of the layout constraint framework, consider the simple truss shown in Fig. 13. The structure shown has three members, two of which are

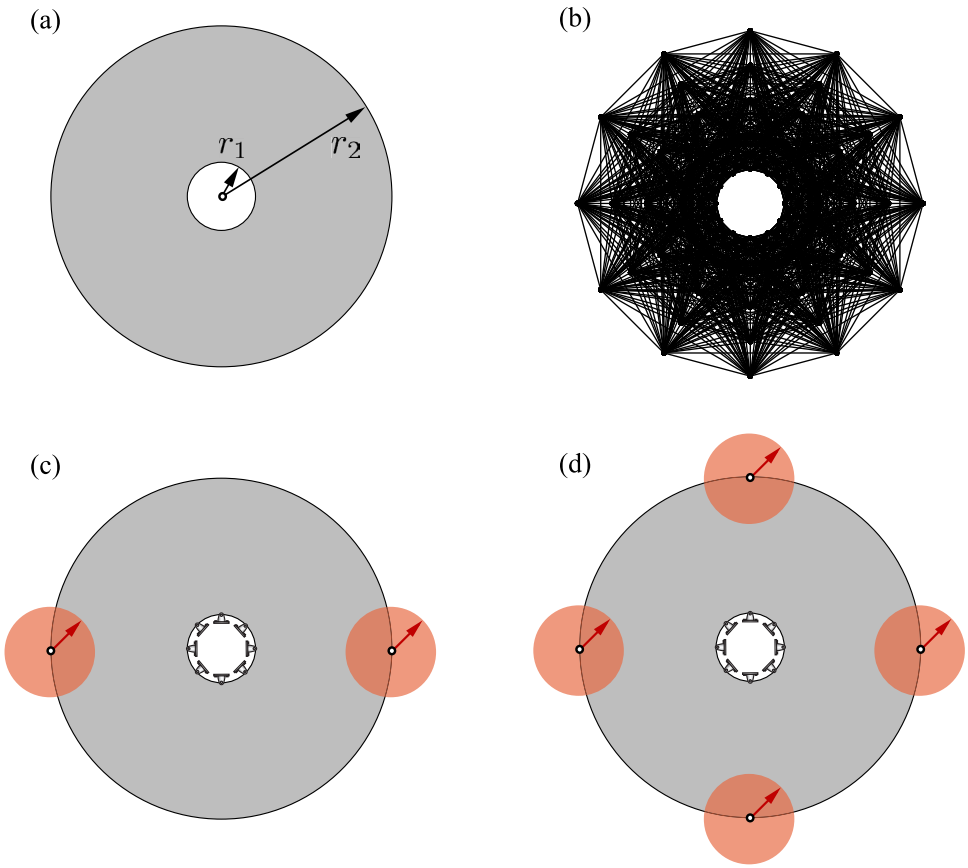

Fig. 9 Disk with multiple varying loads. **a** the geometry of the disk domain; **b** the generated ground structure mesh; **c** case 1 loading and boundary conditions; **d** case 2 loading and boundary conditions

contained in the same LC. For this case we can write Eq. 41 as follows:

$$\begin{bmatrix} x_1 \\ x_2 \\ x_3 \end{bmatrix} = \begin{bmatrix} 1 & 0 \\ 0 & 1 \\ 0 & 1 \end{bmatrix} \begin{bmatrix} y_1 \\ y_2 \end{bmatrix} \tag{42}$$

Here, it is clear to see how the linear mapping is used to correlate the cross-sectional areas to the auxiliary variables such that layout constraint regions are associated with the same design variable. This reduces the number of design variables and enforces regions with the same cross-sectional areas.

Additional details for this problem include a damping strategy implemented in the OC update scheme similarly to Giraldo-Londoño and Paulino (2021).

$$\boldsymbol{y}_k = \xi \boldsymbol{y}_{k-1} + (1-\xi)\boldsymbol{y}_{oc} \tag{43}$$

Here, ξ is the damping parameter, $\boldsymbol{y}_{oc}$ is the vector of design variables calculated by OC, $\boldsymbol{y}_k$ and $\boldsymbol{y}_{k-1}$ are the vectors of design variables damped in iterations k and $k-1$. This was implemented to speed up convergence on some of the hook examples.

Four cases of layout constraints on the hook domain are examined as shown in Fig. 14. The influence of the layout constraints are observed in the optimized structures, which obtain distinct members in the location of the layout constraints. By comparing Case 1 and Case 2 of the layout constraints, we observe that because the inside of the hook requires thicker elements in Case 1, that when we impose a layout constraint on members on the inside of the hook, as in Case 2, the entire region will have a high cross-sectional area. It is observed that radial elements arise naturally in Case 1 and thus the scenario imposing individual radial layout constraints was explored in Case 3. In Case 4, the most number of elements are restricted in a single layout constraint. When comparing the compliance of the optimized structures in Fig. 14c, we see the most optimal of the four structures is Case 1 as expected due to it being subject to the least number of layout constraints. The second most efficient is the structure of Case 3 which took advantage of the naturally arising radial element features in Case 1 by imposing by imposing 18 layout constraints on those areas. The compliance results of Case 2 and Case 4 indicate that poorly chosen layout constraints or one larger layout constraint may lead to drawbacks in structural efficiency.

Furthermore, the results are examined more closely in the histogram in Fig. 15 comparing the normalized cross-sectional areas of the 251 bars in Case 3 associated with layout constraints and the same bars in Case 1. The results in

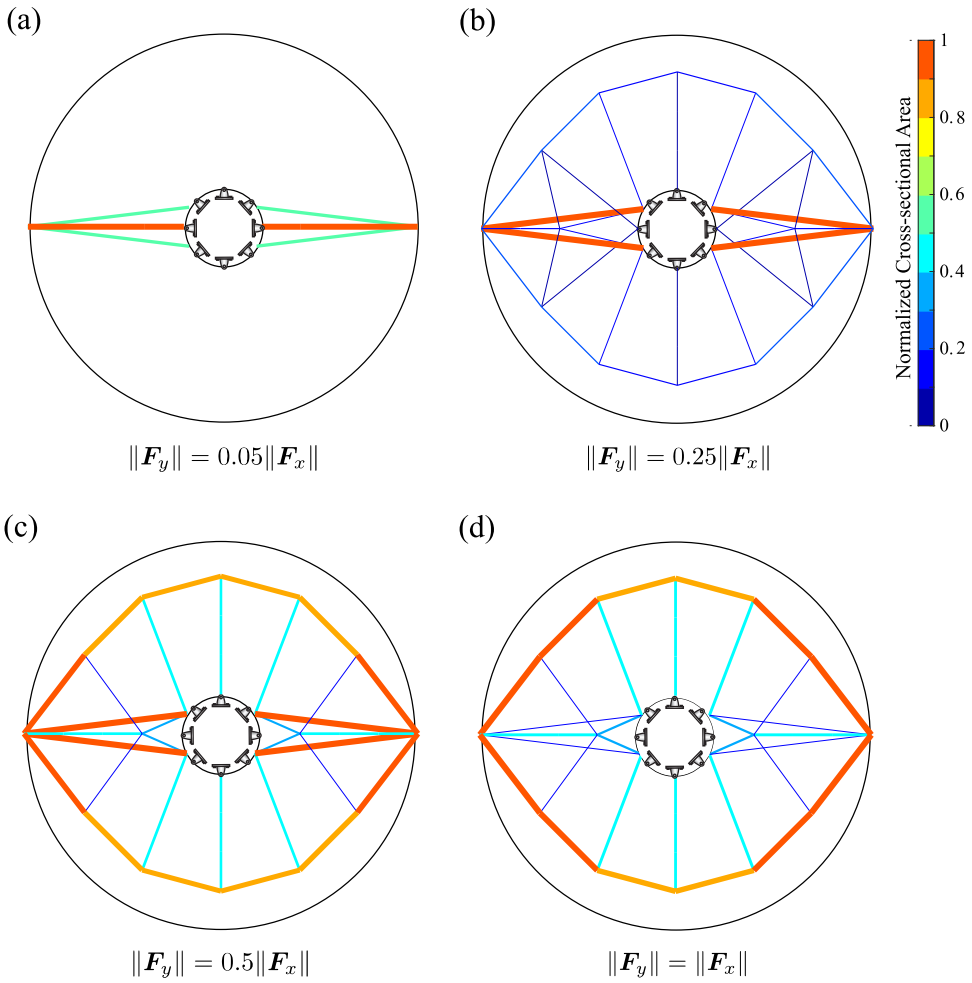

Fig. 10 Results from Case 1 of the disk domain **a** topology resulting from $\|F_y\| = 0.05\|F_x\|$; **b** topology resulting from $\|F_y\| = 0.25\|F_x\|$; **c** topology resulting from $\|F_y\| = 0.5\|F_x\|$; **d** topology resulting from $\|F_y\| = \|F_x\|$

Table 5 Objective values of disk domain examples

Compliance objective value		
	Case 1	Case 2
a	0.63	9.29
b	1.07	10.30
c	2.05	12.06
d	5.81	15.01

the histogram clearly illustrate the benefit of applying layout constraints in the ground structure setting. It is observed in case 1 that the radial bars were already tending toward similar areas in the radial bar regions and by imposing those regions as layout constraints we arrive at element areas with less variation ideal for engineering purposes.

5.6 Circular domain with constrained loading

Here, we present a circular domain with a radius of 5 units with a load applied to the center of the domain, which can vary within the prescribed loading bounds defined by θ_r. Our domain is composed of 110 elements arranged in the way shown in Fig. 16 and four examples are run each with a different constraint on the loading direction. For more information on the example parameters see Table 7.

We present this example due to the symmetries along both the x and y axis. Not only does this invoke the repeated eigenvalues but it also leads to oscillation of the critical load case direction on the bound. Here, we demonstrate that our proposed framework can handle these numerical instabilities; generating results that are robust and consider a range of admissible loading.

In addition, to ensure optimal performance of the MMA optimizer, we impose a normalization on the design variables

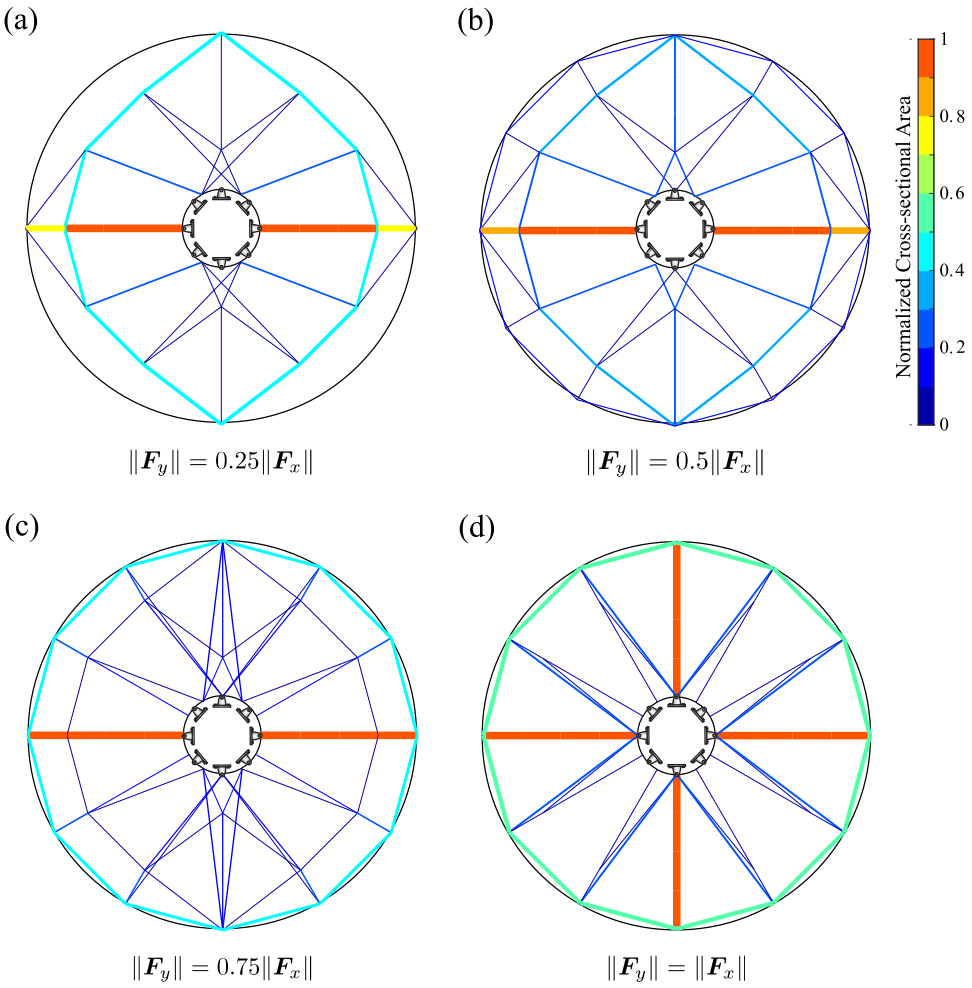

Fig. 11 Results from case 2 of the disk domain **a** topology resulting from $\|\boldsymbol{F}_y\| = 0.25\|\boldsymbol{F}_x\|$; **b** topology resulting from $\|\boldsymbol{F}_y\| = 0.5\|\boldsymbol{F}_x\|$; **c** topology resulting from $\|\boldsymbol{F}_y\| = 0.75\|\boldsymbol{F}_x\|$; **d** topology resulting from $\|\boldsymbol{F}_y\| = \|\boldsymbol{F}_x\|$

such that they lie between $t_{min} = 0.1$ and $t_{max} = 100$. We do this by transforming the design variables by Eq. 44

$$\boldsymbol{x}(\boldsymbol{t}) = a_0 + a_1\boldsymbol{t}, \tag{44}$$

where $\boldsymbol{x}$ is the new set of normalized design variables and $\boldsymbol{t}$ is the original set of design variables. The coefficients a_0 and a_1 are defined as follows:

$$a_0 = -\left(\frac{t_{\min}x_{\max} - t_{\max}x_{min}}{t_{\max} - t_{\min}}\right) \tag{45}$$

and

$$a_1 = \frac{x_{\max} - x_{min}}{t_{\max} - t_{\min}}. \tag{46}$$

This normalization also impacts the sensitivity analysis by a factor of a_1 as shown in Eq. 47:

$$\frac{\partial x_i}{\partial t_i} = a_1, \tag{47}$$

where index i refers to the pertinent variable. The results of this example are shown in Fig. 17 with four different topologies each corresponding to a different constraint on the

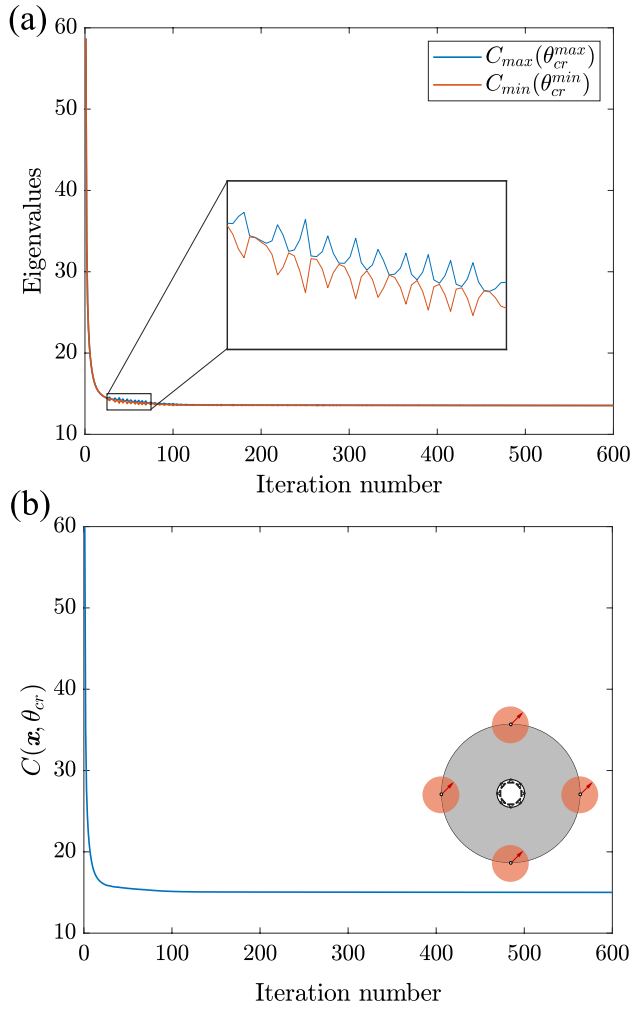

Fig. 12 Convergence details of the case 2 of the Disk domain with $\|\boldsymbol{F}_y\| = \|\boldsymbol{F}_x\|$ **a** convergence history of the eigenvalues; **b** convergence history of the objective function

Table 6 Topology optimization parameters for the Hook domain

Elastic modulus, E	1×10^4
Number of GS bars, N_{bar}	2,687
Initial area, x_{ini}	9.05×10^{-5}
Maximum area, x_{max}	1.11
Minimum area, x_{min}	1×10^{-12}
Volume limit, V_{max}	1
Move parameter, γ	9.05×10^{-5}
Convergence tolerance	1×10^{-8}
End filter, α_f	10^{-4}
Damping parameter, ξ	0.7

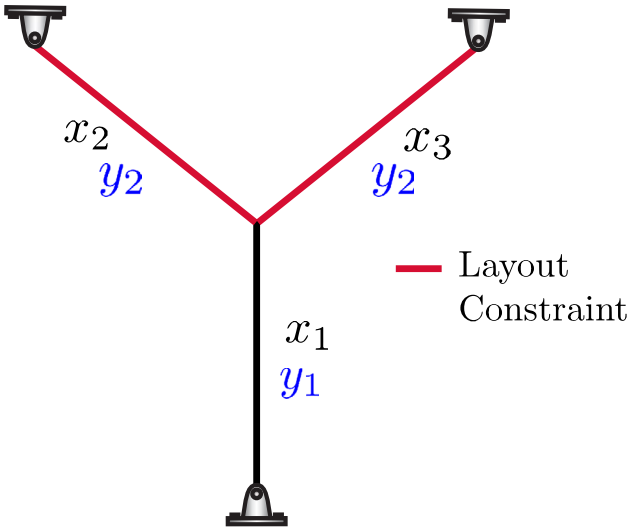

Fig. 13 Simple truss illustrating the LC constraint concept

loading direction. We observe that as the range on θ increases so does the number of bars in a fan like fashion. The thin bars that lie outside of the load range are placed there as a result of the robust topology optimization framework and the user specified end filter. In the case where $\theta_r = 0$, in Fig. 17, the resulting topology is equivalent to what is achieved in the nominal case, where the load is applied in the x direction. The final compliance for these examples increases as the range of admissible loads increases, these values are shown in Table 8. To view the convergence plots of these examples see Fig. 18. It is observed that as the range of admissible angles decreases it takes more iterations to converge, this is a result from the oscillation of the critical load case on the bound.

6 Conclusion

In this paper, a deterministic RTO approach is presented for ground structure networks. The optimization problem of finding the critical load case direction associated with the maximum compliance was shown to be equivalent to a maximum eigenvalue problem. Here, we present an approach for treating the maximum eigenvalue function in an RTO framework by the μ smooth maximum regularization function to treat the non-smoothness of the objective function.

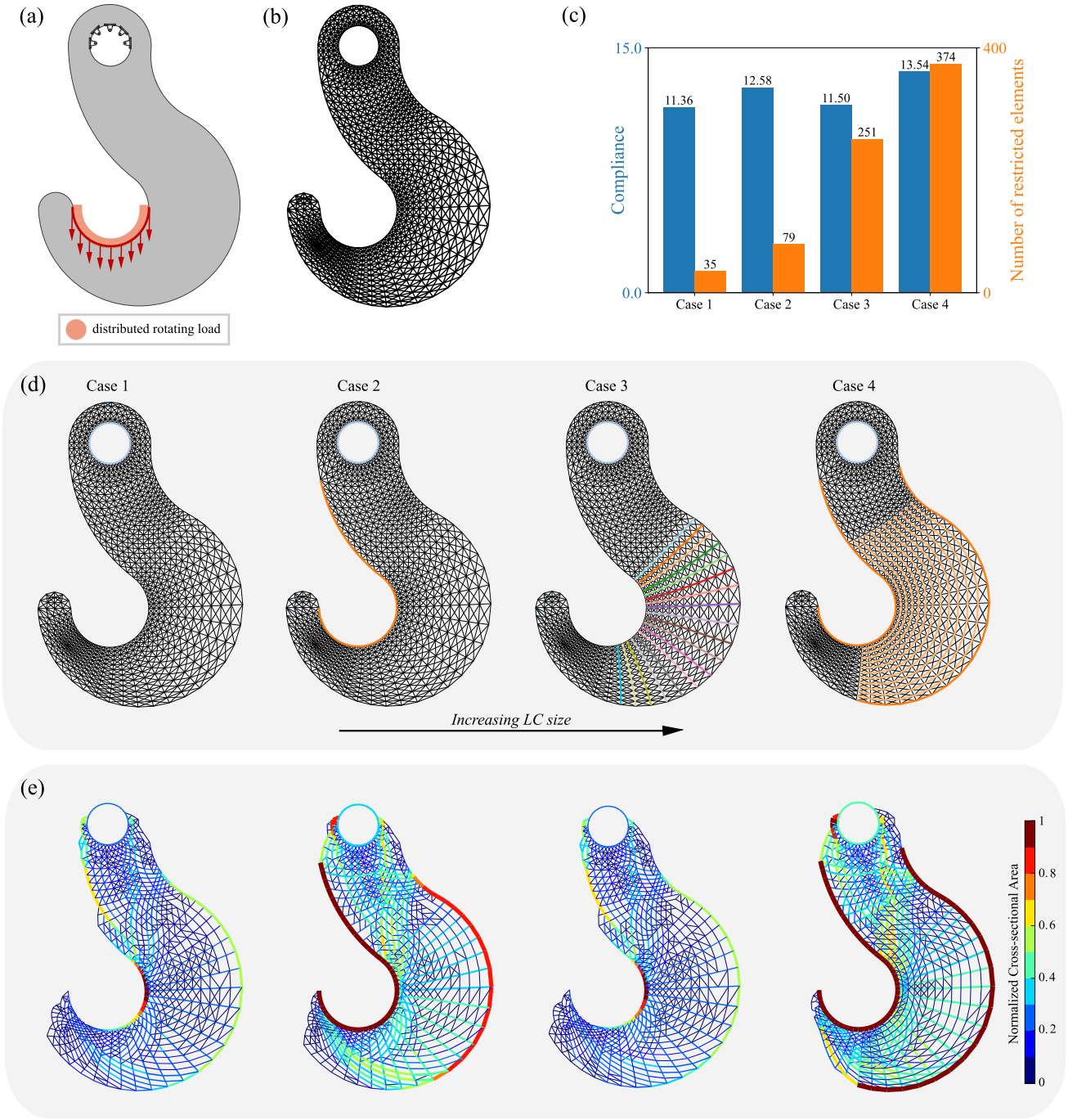

Fig. 14 Results of the Hook domain **a** loading (shown in red) and boundary conditions; **b** ground structure mesh; **c** the number of total restricted elements in each layout constraint case; **d** layout constraint designs for the four cases (each color corresponding to a layout constraint) and **e** their resulting optimized structures

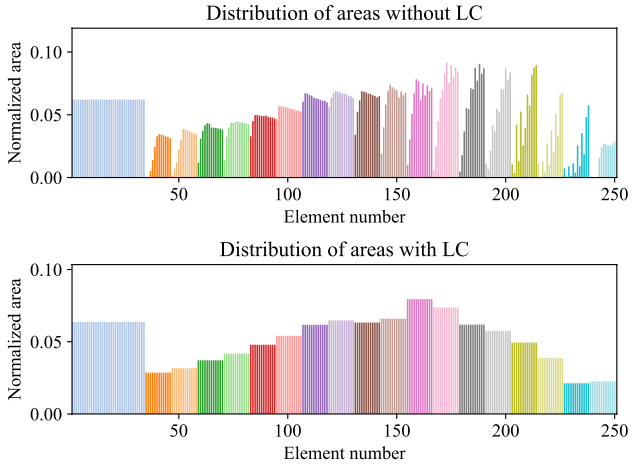

Fig. 15 Histogram of the normalized cross-sectional areas for select elements in Case 1 (top) and for the same elements in Case 3 (bottom)

Table 7 Topology optimization parameters for the circular domain

Elastic modulus, E	1
Number of GS bars, N_{bar}	110
Initial area, x_{ini}	1.8349×10^{-3}
Maximum area, x_{max}	1.0×10^{-12}
Minimum area, x_{min}	0.2
Volume limit, V_{max}	1
Convergence tolerance	1×10^{-8}
End filter, α_f	1.0×10^{-4}

Table 8 Objective values of the Circular domain examples subject to a range of admissible loads

Circular domain objective value		
	θ_r	Compliance
a	0	25.00
b	$\pi/1800$	25.35
c	$\pi/36$	29.44
d	$\pi/6$	46.75

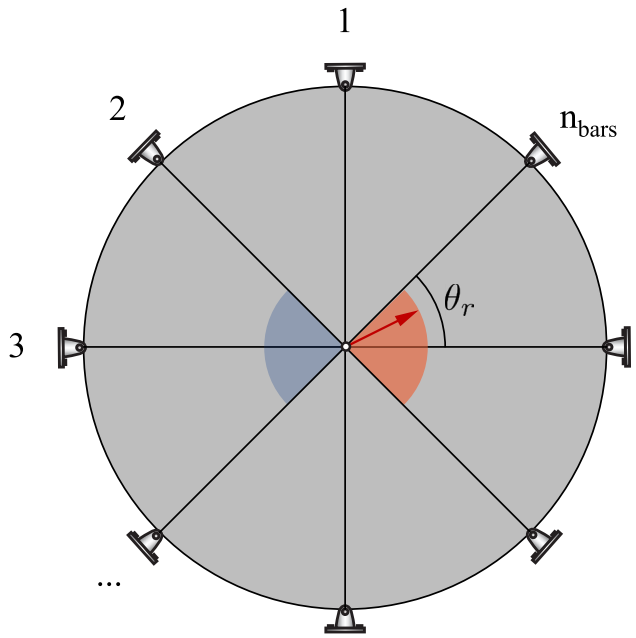

Fig. 16 The loading and boundary conditions of the circular domain subject to constrained loading

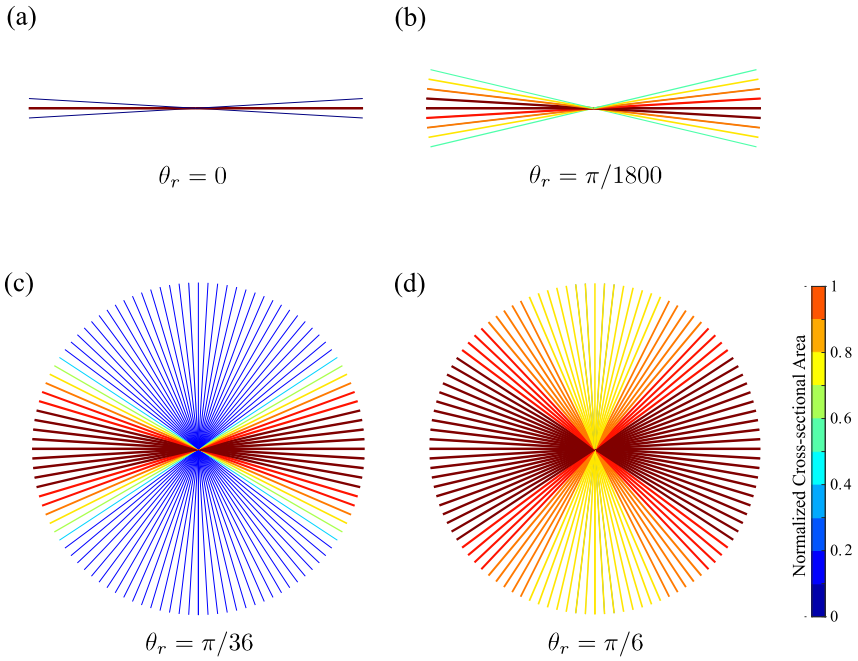

Fig. 17 The results of the circular domain subject to constrained loading for **a** the case when $\theta_r = 0$; **b** the case where $\theta_r = \pi/1800$; **c** the case when $\theta_r = \pi/36$; **d** the case when $\theta_r = \pi/6$

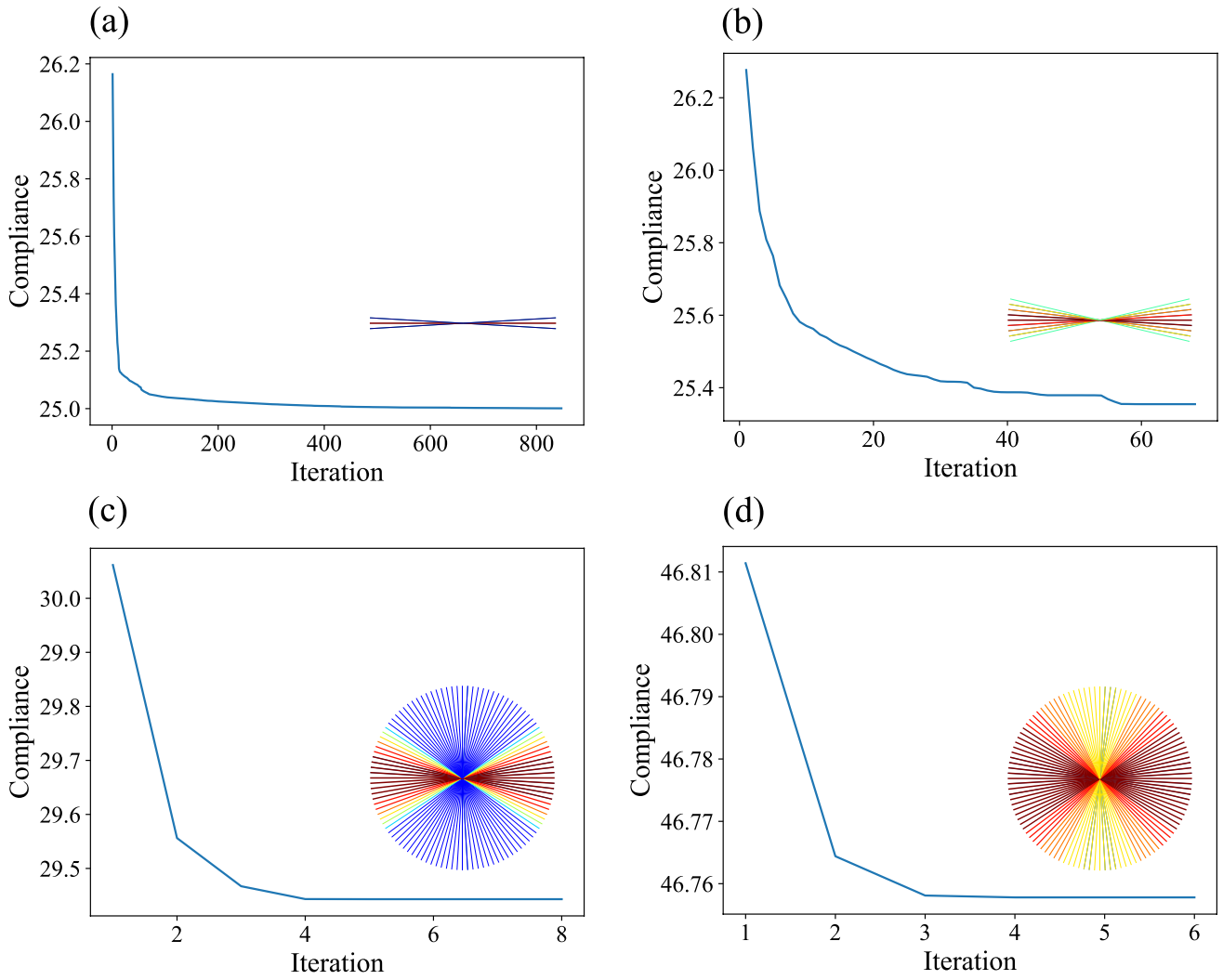

Fig. 18 The convergence of the circular domain subject to constrained loading for **a** the case when $\theta_r = 0$; **b** the case where $\theta_r = \pi/1800$; **c** the case when $\theta_r = \pi/36$; **d** the case when $\theta_r = \pi/6$

The results confirm our approach for designing structures with low compliance for all possible load directions. The structures are shown to be exceedingly more reliable in terms of compliance performance for all possible load case directions versus the conventional topology optimization considering a single load case direction. The flexibility and control of the loading parameterization is shown to describe a wide variety of loading domains including: elliptical load domains, multiple varying point loads, constrained varying loads, and distributed rotating loads. We conclude that the proposed framework is an effective approach when considering loads with rotating direction or uncertainty in the direction to design truss structures that are both efficient and robust.

Appendix A

Nomenclature

$\boldsymbol{A}$	Real symmetric matrix
$\boldsymbol{B}$	Matrix with nominal loads
C	Compliance
C_{max}	Maximum compliance
C_{min}	Minimum compliance
E	Young's modulus
f_μ	μ-regularization function
f_p	P-norm regularization function
$\boldsymbol{F}_x$	Basis load vector in x direction
$\boldsymbol{F}_y$	Basis load vector in y direction
$\boldsymbol{F}$	Load vector
FEA	Finite element analysis

g	Volume constraint
$\mathcal{L}$	Lagrangian
$\boldsymbol{L}$	Vector of bars lengths
$\boldsymbol{n}$	Unit vector with load direction
OC	Optimality Criteria method
$\boldsymbol{P}$	Binary mapping matrix
p	P-norm regularization parameter
RTO	Robust topology optimization
$\boldsymbol{r}$	Vector with worst load case direction
$\boldsymbol{T}$	Compliance matrix
$\boldsymbol{U}$	Displacements vector
$\boldsymbol{U}_x$	Displacements vector in x direction
$\boldsymbol{U}_y$	Displacements vector in y direction
$\boldsymbol{v}_i$	Eigenvector i of a matrix
V_{max}	Maximum volume
$\boldsymbol{x}$	Vector of design variables
x_{ini}	Cross-sectional area of element i
x_{min}	Minimum design variables magnitude
x_{max}	Maximum design variables magnitude
$\boldsymbol{y}$	Vector of auxiliary variables
α_f	Filter cutoff parameter
β	Dimensionless μ-regularization parameter
λ	Lagrange multiplier
λ_i	Eigenvalue i of a matrix
θ	Load angle
θ_r	Load angle range
θ_{rot}	Rotation angle of load domain basis
θ^{cr}_{min}	Critical angle of minimum compliance
θ^{cr}_{max}	Critical angle of maximum compliance

Appendix B

P-norm regularization

In addition to the μ-regularization function other regularization techniques can be used to satisfy the requirements made in Remark 1. One of these regularization functions is the p-norm function, which can be expressed in terms of eigenvalues as follows:

$$f_p(\lambda_1(\boldsymbol{x}), \lambda_2(\boldsymbol{x})) = \left(\lambda_1{}^p + \lambda_2{}^p\right)^{1/p}. \tag{B1}$$

The p-norm is a smooth maximum regularization function that will more closely approximate the $\max(\lambda_1, \lambda_2)$ as $p \to \infty$. Because the p-norm is constructed by a summation terms of the eigenvalues it is observed that the function is smooth and the derivative exists. To further illustrate this for the repeated eigenvalue case, the derivative of the p-norm function is derived analytically.

$$\frac{d}{d\boldsymbol{x}}[f_p(\lambda_1(\boldsymbol{x}), \lambda_2(\boldsymbol{x}))] = \frac{\partial f_p}{\partial \lambda_1}\frac{\partial \lambda_1}{\partial \boldsymbol{x}} + \frac{\partial f_p}{\partial \lambda_2}\frac{\partial \lambda_2}{\partial \boldsymbol{x}} \tag{B2}$$

By taking the partial derivatives of the function with respect to the eigenvalues, we arrive at the following expressions:

$$\frac{\partial f_p}{\partial \lambda_1} = \left(\lambda_1^p + \lambda_2^p\right)^{\frac{1}{p}-1} \lambda_1^{p-1} \tag{B3}$$

$$\frac{\partial f_p}{\partial \lambda_2} = \left(\lambda_1^p + \lambda_2^p\right)^{\frac{1}{p}-1} \lambda_2^{p-1} \tag{B4}$$

By taking $\lambda_1 = \lambda_2$ for the repeated eigenvalue case, we arrive at the following simplification:

$$\frac{\partial f_p}{\partial \lambda_1} = \frac{\partial f_p}{\partial \lambda_2} = \left(2\lambda_1^p\right)^{\frac{1}{p}-1} \lambda_1^{p-1} \tag{B5}$$

With this information, Eq. B2 can be simplified and composed of summations of the derivatives of eigenvalues. Under the implications made in Remark 1, the summations of repeated eigenvalues are continuous and thus their derivatives exist. Thus, allowing us to have accurate sensitivity information for all components of the p-norm function.

$$\frac{d}{d\boldsymbol{x}}[f_p(\lambda_1(\boldsymbol{x}), \lambda_2(\boldsymbol{x}))] = \frac{\partial f_p}{\partial \lambda_1}\left(\frac{\partial \lambda_1}{\partial \boldsymbol{x}} + \frac{\partial \lambda_2}{\partial \boldsymbol{x}}\right) \tag{B6}$$

Appendix C

Eigenvalue problem for the spherical load case

The equations shown here are presented to set up the optimization problem for the three-dimensional case. We begin by defining the load parameterization through relating the cartesian coordinates to the spherical polar coordinates by

$$\begin{aligned} x &= \sin\phi\cos\theta \\ y &= \sin\phi\sin\theta \\ z &= \cos\phi, \end{aligned} \tag{C7}$$

where $\theta \in [-\pi, \pi]$ and $\phi \in [0, \pi]$. The loading parameterization for the 3-D case representing a spherical load may be expressed as follows:

$$F(\phi, \theta, \boldsymbol{x}) = \boldsymbol{F}_x \sin\phi\cos\theta + \boldsymbol{F}_y \sin\phi\sin\theta + \boldsymbol{F}_z \cos\phi \tag{C8}$$

The vectors $\boldsymbol{F}_x$, $\boldsymbol{F}_y$, and $\boldsymbol{F}_z$ correspond to the basis vectors of the spherical loading description. Similarly to the two-dimensional case, the three-dimensional case for finding the critical load direction for the worst case compliance

is also equivalent to a maximum eigenvalue problem. The compliance objective for this problem may be expressed as follows:

$$C(\boldsymbol{x}, \theta) = \boldsymbol{n}^T \boldsymbol{T} \boldsymbol{n}, \tag{C9}$$

where

$$\boldsymbol{n} = \begin{bmatrix} \sin\phi\cos\theta \\ \sin\phi\sin\theta \\ \cos\phi \end{bmatrix} \tag{C10}$$

$$\boldsymbol{T} = \begin{bmatrix} \boldsymbol{U}_x\boldsymbol{K}\boldsymbol{U}_x & \boldsymbol{U}_x\boldsymbol{K}\boldsymbol{U}_y & \boldsymbol{U}_x\boldsymbol{K}\boldsymbol{U}_z \\ \boldsymbol{U}_y\boldsymbol{K}\boldsymbol{U}_x & \boldsymbol{U}_y\boldsymbol{K}\boldsymbol{U}_y & \boldsymbol{U}_y\boldsymbol{K}\boldsymbol{U}_z \\ \boldsymbol{U}_z\boldsymbol{K}\boldsymbol{U}_x & \boldsymbol{U}_z\boldsymbol{K}\boldsymbol{U}_y & \boldsymbol{U}_z\boldsymbol{K}\boldsymbol{U}_z \end{bmatrix}. \tag{C11}$$

Equivalent to Eq. 6, the optimization problem for determining the worst case loading direction for the spherical load is a maximum eigenvalue problem. The eigenvalues of the compliance matrix $\boldsymbol{T}$ correlate to the principal worst case compliances and their corresponding eigenvector to the critical loading directions.

Appendix D

Sensitivity analysis of the layout constraint framework

The sensitivity of the objective function in Eq. (40) is obtained by applying the chain rule to the expression.

$$\frac{\partial C}{\partial \boldsymbol{y}} = \frac{\partial C}{\partial \boldsymbol{x}} \frac{\partial \boldsymbol{x}}{\partial \boldsymbol{y}}. \tag{D12}$$

In index notation, we write the following:

$$x_i = P_{ij} y_j \tag{D13}$$

$$\frac{\partial x_i}{\partial y_k} = P_{ij} \frac{\partial y_j}{\partial y_k} \tag{D14}$$

Considering that $\partial y_j / \partial y_k = \delta_{jk}$ and $P_{ij}\delta_{jk} = P_{ik}$ we obtain

$$\frac{\partial \boldsymbol{x}}{\partial \boldsymbol{y}} = \boldsymbol{P}^\top. \tag{D15}$$

Substituting Eqs. (D15) in (D12), we arrive at the following:

$$\frac{\partial C}{\partial \boldsymbol{y}} = \boldsymbol{P}^\top \frac{\partial C}{\partial \boldsymbol{x}} \tag{D16}$$

Similarly for the constraint function we have

$$\frac{\partial g}{\partial \boldsymbol{y}} = \boldsymbol{P}^\top \frac{\partial g}{\partial \boldsymbol{x}}. \tag{D17}$$

Acknowledgements The authors acknowledge the financial support given by NSF grant No. 2105811 and the Brazilian agency CNPq (National Council for Research and Development). We are also grateful for the support granted by the Margareta Engman Augustine endowment at Princeton University.

Declarations

Conflict of interest The authors declare that they have no Conflict of interest.

Replication of results To reproduce the numerical results, the authors refer the reader to the input parameters table for each example as well as the optimization formulation in Sect. 3, which discusses the implementation in detail.

References

Bae KR, Wang S (2002) Reliability-based topology optimization. In: 9th AIAA-ISSMO symposium on multidisciplinary analysis and optimization, p 5542

Bendsøe MP (1995) Optimization of structural topology, shape, and material, vol 414. Springer, Cham

Bendsøe MP, Kikuchi N (1988) Generating optimal topologies in structural design using a homogenization method. Comput Methods Appl Mech Eng 71(2):197–224

Bendsoe MP, Sigmund O (2013) Topology optimization: theory, methods, and applications. Springer, Cham

Ben-Tal A, Nemirovski A (1997) Robust truss topology design via semidefinite programming. SIAM J Optim 7(4):991–1016

Ben-Tal A, El Ghaoui L, Nemirovski A (2009) Robust optimization, vol 28. Princeton University Press, Princeton

Beyer HG, Sendhoff B (2007) Robust optimization-a comprehensive survey. Comput Methods Appl Mech Eng 196(33–34):3190–3218

Biswas K, Kumar S, Banerjee S, Pandey AK (2021) Smu: Smooth activation function for deep networks using smoothing maximum technique. Preprint at http://arxiv.org/abs/2111.04682

Chandu SV, Grandhi RV (1995) General purpose procedure for reliability based structural optimization under parametric uncertainties. Adv Eng Softw 23(1):7–14

Chen X, Qi H, Qi L, Teo K-L (2004) Smooth convex approximation to the maximum eigenvalue function. J Global Optim 30(2):253–270

Cherkaev E, Cherkaev A (2008) Minimax optimization problem of structural design. Comput Struct 86(13–14):1426–1435

Da Silva G, Beck AT, Cardoso EL (2018) Topology optimization of continuum structures with stress constraints and uncertainties in loading. Int J Numer Methods Eng 113(1):153–178

De S, Hampton J, Maute K, Doostan A (2020) Topology optimization under uncertainty using a stochastic gradient-based approach. Struct Multidisc Optim 62(5):2255–2278

Dunning PD, Kim HA (2013) Robust topology optimization: minimization of expected and variance of compliance. AIAA J 51(11):2656–2664

Dunning PD, Ovtchinnikov E, Scott J, Kim HA (2016) Level-set topology optimization with many linear buckling constraints using an efficient and robust eigensolver. Int J Numer Methods Eng 107(12):1029–1053

Giraldo-Londoño O, Paulino GH (2021) PolyDyna: a matlab implementation for topology optimization of structures subjected to dynamic loads. Struct Multidisc Optim 64(2):957–990

Gravesen J, Evgrafov A, Nguyen DM (2011) On the sensitivities of multiple eigenvalues. Struct Multidisc Optim 44(4):583–587
Holmberg E, Thore CJ, Klarbring A (2015) Worst-case topology optimization of self-weight loaded structures using semi-definite programming. Struct Multidisc Optim 52(5):915–928
Holmberg E, Thore CJ, Klarbring A (2017) Game theory approach to robust topology optimization with uncertain loading. Struct Multidisc Optim 55(4):1383–1397
Jansen M, Lombaert G, Schevenels M (2015) Robust topology optimization of structures with imperfect geometry based on geometric nonlinear analysis. Comput Methods Appl Mech Eng 285:452–467
Jensen HA (2005) Design and sensitivity analysis of dynamical systems subjected to stochastic loading. Comput Struct 83(14):1062–1075
Johnson SG (2007) The NLopt nonlinear-optimization package. https://github.com/stevengj/nlopt
Kharmanda G, Olhoff N, Mohamed A, Lemaire M (2004) Reliability-based topology optimization. Struct Multidisc Optim 26(5):295–307
Lewis AS, Overton ML (1996) Eigenvalue optimization. Acta Numer 5:149–190
Maute K, Frangopol DM (2003) Reliability-based design of mems mechanisms by topology optimization. Comput Struct 81(8–11):813–824
Michell AGM (1904) Lviii the limits of economy of material in frame-structures. London Edinburgh Philos Mag J Sci 8(47):589–597
Nishioka A, Kanno Y (2023) Smoothing inertial method for worst-case robust topology optimization under load uncertainty. Struct Multidisc Optim 66(4):82
Overton ML, Womersley RS (1995) Second derivatives for optimizing eigenvalues of symmetric matrices. SIAM J Matrix Anal Appl 16(3):697–718
Reddy MV, Grandhi RV, Hopkins DA (1994) Reliability based structural optimization: a simplified safety index approach. Comput Struct 53(6):1407–1418
Rozvany GI (2009) A critical review of established methods of structural topology optimization. Struct Multidisc Optim 37(3):217–237
Schuëller GI, Jensen HA (2008) Computational methods in optimization considering uncertainties-an overview. Comput Methods Appl Mech Eng 198(1):2–13
Senhora FV, Menezes IF, Paulino GH (2023) Topology optimization with local stress constraints and continuously varying load direction and magnitude: towards practical applications. Proc R Soc A 479(2271):20220436
Seyranian AP, Lund E, Olhoff N (1994) Multiple eigenvalues in structural optimization problems. Struct Optim 8(4):207–227
Shapiro A, Fan MK (1995) On eigenvalue optimization. SIAM J Optim 5(3):552–569
Sigmund O, Maute K (2013) Topology optimization approaches. Struct Multidisc Optim 48(6):1031–1055
Stromberg LL, Beghini A, Baker WF, Paulino GH (2011) Application of layout and topology optimization using pattern gradation for the conceptual design of buildings. Struct Multidisc Optim 43:165–180
Svanberg K (2002) A class of globally convergent optimization methods based on conservative convex separable approximations. SIAM J Optim 12(2):555–573
Thanedar PB, Kodiyalam S (1992) Structural optimization using probabilistic constraints. Struct Optim 4(3):236–240
Thore CJ, Holmberg E, Klarbring A (2017) A general framework for robust topology optimization under load-uncertainty including stress constraints. Comput Methods Appl Mech Eng 319:1–18
Torii AJ, Faria JRD (2017) Structural optimization considering smallest magnitude eigenvalues: a smooth approximation. J Braz Soc Mech Sci Eng 39(5):1745–1754
Zegard T, Paulino GH (2014) Grand–ground structure based topology optimization for arbitrary 2d domains using matlab. Struct Multidisc Optim 50:861–882
Zhao J, Wang C (2014) Robust topology optimization under loading uncertainty based on linear elastic theory and orthogonal diagonalization of symmetric matrices. Comput Methods Appl Mech Eng 273:204–218